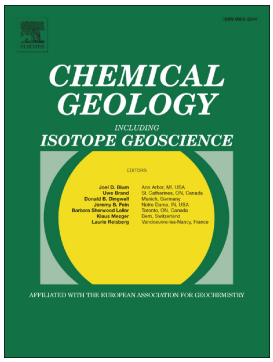

Age disequilibrium between zircon and their granitoid hosts caused by intracrustal reworking: Nd-Hf-Ar isotope evidence of Archean Granitoids from Barberton Mountain Land (Kaapvaal craton, South Africa)

Ilka C. Kleinhanns, Thomas F. Nägler, Igor M. Villa, Jan D. Kramers

PII: S0009-2541(21)00073-5

DOI: https://doi.org/10.1016/j.chemgeo.2021.120129

Reference: CHEMGE 120129

To appear in: *Chemical Geology*

Received date: 1 October 2020

Revised date: 10 February 2021

Accepted date: 12 February 2021

Please cite this article as: I.C. Kleinhanns, T.F. Nägler, I.M. Villa, et al., Age disequilibrium between zircon and their granitoid hosts caused by intracrustal reworking: Nd-Hf-Ar isotope evidence of Archean Granitoids from Barberton Mountain Land (Kaapvaal craton, South Africa), *Chemical Geology* (2021), https://doi.org/10.1016/j.chemgeo.2021.120129

Age disequilibrium between zircon and their granitoid hosts caused by intracrustal reworking: Nd-Hf-Ar isotope evidence of Archean Granitoids from Barberton Mountain Land (Kaapvaal craton, South Africa)

Ilka C. Kleinhanns[1,2*], Thomas F. Nägler[2], Igor M. Villa[2] & Jan D. Kramers[3,2],

[1] GUZ, Department of Geological Sciences, University of Tuebingen, Schnarrenbergstrasse 94-96, D-72076 Tuebingen, Germany

[2] Institute of Geological Sciences, University of Bern, Baltzerstrasse 1+3, CH-3012 Bern, Switzerland

[3] Department of Geology, University of Johannesburg, Auckland Park 2006, Johannesburg, South Africa

*Corresponding author:

email: kleinhanns@ifg.uni-tuebingen.de, fon: +49 (0)7071 29 78908

Abstract

The degree of early Archean terrestrial differentiation into mantle and crust is long debated. A number of studies rely on bulk rock Hf and Nd isotope data to gain further insight. Here we present Hf-Nd data from two igneous basements suites of Barberton Mountain Land, namely a tonalite-trondhjemite-granodiorite (TTG) and granodiorite-granite-monzogranite (GGM) suite to further decipher crust formation and its timing in the Archaean. TTG show high initial ε(Hf) and ε(Nd) if corrected using their respective U-Pb zircon ages that can be interpreted in two ways: (i) early differentiation of bulk silicate Earth or (ii) overcorrection of these data caused by decoupling of zircon from the 'zircon-free' bulk rock due to metamorphic overprint. Indeed, regional metamorphism affected the early TTG ca. 250 Ma after their emplacement and disturbed their bulk rock Hf and Nd systematics. Correction of bulk rock Hf and Nd data to the age of metamorphism yields values between +0.9 and -6.2 and from –1.3 to –4.3, respectively, thus indicating open-system behaviour. Lu-Hf and Sm-Nd mineral isochron ages of two TTG plutons are significantly younger than their corresponding U-Pb zircon age, but agree within uncertainty perfectly with external age

constraints for the age of the metamorphic overprint. The same accounts for the ^{40}Ar-^{39}Ar systematics of the investigated plutons. Amphibole samples consist of a mixture of heterochemical generations that yield ages that are both older and younger than the metamorphic overprint at 3.2 Ga. The metamorphic minerals in each plutons provide a highly divergent age information from the coexisting zircon. Hence, the positive ε(Nd) and ε(Hf)-values that resulted from age-correction to the respective U-Pb zircon age are most probably over-corrected. Finally, if all data is age-corrected to the metamorphic overprint all samples agree with models for the Nd-Hf isotopic evolution in the mantle that do not require a large-scale early differentiation of Earth into enriched and depleted reservoirs. Mantle extraction ages (T_{DM}) of TTG are interpreted as minimum ages for the generation of felsic Archaean crust whereas T_{DM} of GGM are interpreted as maximum ages for the last major crust growth episode in the Barberton Mountain Land.

Keywords

Archean, continental crust, Hf, Nd, zircon, age heterogeneity, Barberton

1. Introduction

The complex differentiation history of the Earth has led to the formation of distinct geochemical reservoirs within our planet. Knowledge about processes within these reservoirs and interaction between them is crucial for a better understanding of Earth's recycling engine and its influence on the distinct reservoirs (Hofmann, 1988; Kamber and Collerson, 2000; Macdonald et al., 2000). This global recycling system was active as early as 3.8 Ga as evidenced by ^{142}Nd-anomalies in early Archaean crustal rocks (Caro et al., 2006; Schneider et al., 2018) and is reasonably well understood for post-Archaean geological time. With regard to the mid- and early Archaean, Hf and Nd isotope signatures

in bulk rocks have been widely applied to assess crust formation processes and their timing. The interpretation of results, however, is highly debated (e.g. (Bennett et al., 1993; Bowring and Housh, 1995; Vervoort et al., 1996; Moorbath et al., 1997; Kamber et al., 1998; Bowring and Williams, 1999; Blichert-Toft and Frei, 2001; Whitehouse et al., 2001; Schoene et al., 2009; Hoffmann et al., 2010; Hoffmann et al., 2011; Guitreau et al., 2012; Kröner et al., 2014; Tang et al., 2014; Payne et al., 2016; Szilas et al., 2016; Huang et al., 2019; Moyen et al., 2019; Laurent et al., 2020). Some of these contradictions are solved by the addition of coupled zircon U-Pb-Hf-O isotope data (e.g. (Hawkesworth and Kemp, 2006; Kemp et al., 2006; Zeh et al., 2009; Hoffmann et al., 2010; Kemp et al., 2010; Hiess and Bennett, 2016; Payne et al., 2016; Vervoort and Kemp, 2016) that are extremely valuable in characterising the source composition and the timing of extraction of melts parental to granitoids. To assess the bulk rock granitoid post-emplacement history, zircons may however not be the perfect choice since they are very resistant to later metamorphic overprint or develop heterogeneous (isotope) geochemical signatures leading even to a de-coupling from 'zircon-free' bulk rock (Mezger and Krogstad, 1997; Cherniak and Watson, 2003; Kröner et al., 2014; Tang et al., 2014; Hiess and Bennett, 2016; Payne et al., 2016; Rubatto, 2017; Huang et al., 2019). Thus, knowledge about possible age discordance between zircon and its host rock is of vital importance for interpretation of time-corrected bulk rock Hf and Nd isotope data.

To address this problem, we investigated bulk rock Sm-Nd and Lu-Hf isotope compositions of granitoids from the Archaean Barberton Mountain Land (BML, South Africa). This region comprises two suites of granitoids, a TTG suite, and a more potassic granodiorite-granite-monzogranite (GGM) suite that intrudes the former (Kamo and Davis, 1994; Lowe, 1999; Schoene et al., 2009; Anhaeusser, 2010; Schoene and Bowring, 2010; Sanchez-Garrido et al., 2011; Kröner et al., 2018; Moyen et al., 2019; Wang et al., 2020). The BML TTGs are well-suited for studying the impact of later metamorphic overprint on

the radiogenic isotope systematics since a major event effected the BML at ca. 3.2 Ga (Dziggel et al., 2002; Stevens et al., 2002; Kisters et al., 2003; Dziggel et al., 2005; Dziggel et al., 2006; Schoene and Bowring, 2010; Lana et al., 2011; Kröner et al., 2018; Wang et al., 2020) that is ca. 250 Ma younger than the emplacement of the early TTG at ~3.45 Ga (Kamo and Davis, 1994; De Ronde and Kamo, 2000; Poujol et al., 2003; Moyen et al., 2019; Laurent et al., 2020; Wang et al., 2020). In the late TTG that were emplaced roughly at the time of this metamorphic event at ~ 3.2 Ga (e.g. Kamo and Davis (1994), Poujol et al. (2003), Schoene et al. (2008) and Wang et al. (2020)) and the GGM, which intruded at ~ 3.1 Ga (e.g. Kamo and Davis (1994) and Poujol et al. (2003)), no large later overprint is observed (Schoene et al., 2008).

In order to investigate the effect of the 3.2 Ga event on the radiogenic isotope systematics of the older TTG, we obtained Sm-Nd and Lu-Hf data of various mineral phases of two of these plutons (Theespruit and Steynsdorp) to test for possible disequilibria of these isotope tracers between different minerals. As a corollary to the mineral Sm-Nd and Lu-Hf isochron ages, ^{40}Ar-^{39}Ar ages on amphiboles were determined for the same two TTG.

2. Geological background

The Barberton Mountain Land (BML, Fig. 1) is a well-studied Paleoarchean region located in the south-eastern Kaapvaal craton, South Africa. Apart from the well-known Barberton greenstone belt, it consists of distinct granitoid suites surrounding and intruding the greenstone remnants ((Kamo and Davis, 1994; Lowe, 1999; Dziggel et al., 2002; Dziggel et al., 2006; Schoene et al., 2009; Anhaeusser, 2010; Kröner et al., 2014; Kröner et al., 2018; Moyen et al., 2019; Laurent et al., 2020) among many others).

The TTG are discriminated into different groups based on their intrusion age and local occurrence, which are the Stolzburg (3.50-3.45 Ga), the Kaap Valley (3.23 Ga) and the

Badplaas domains (3.29-3.23 Ga) (Kisters et al., 2010) corresponding to TTG1&2, TTG3b and TTG3a of Moyen et al. (2019), respectively.

The Stolzburg domain is located to the south of the BGB and comprises the oldest TTGs within BML, namely the Stolzburg, Theespruit and Steynsdorp plutons with emplacement ages > 3440 Ma (Kamo and Davis, 1994; Poujol et al., 2003; Moyen et al., 2019; Laurent et al., 2020). The domain underwent amphibolite-facies metamorphism in the course of a larger event (D2) that affected the BML at ca. 3.2 Ga, and evidences deep-crustal burial of the Stolzburg domain ca. 250 Ma after formation (Dziggel et al., 2002; Stevens et al., 2002; Kisters et al., 2003; Dziggel et al., 2005; Dziggel et al., 2006; Schoene and Bowring, 2010; Lana et al., 2011; Kröner et al., 2018). Pressure-temperature estimates for the Stolzburg domain vary from 7.5 kbar and ca. 550°C in the north to 10-12 kbar and 650-700°C at the southern margin (Dziggel et al., 2002; Diener et al., 2005). Additionally, the Stolzburg pluton shows a second and younger zircon generation with an age of 3237-3255 Ma (Kamo and Davis, 1994) that presumably is connected to this burial event. The high-grade metamorphic event is further evident through U/Pb ages of ~3.2 Ga derived from apatite, rutile and titanite from Stolzburg domain TTG (Kamo and Davis, 1994; Schoene et al., 2008).

The Badplaas domain is located to the west of the Stolzburg domain. This domain is characterised by a more complex structural and polyphase history (Kisters et al., 2010). The Kaap Valley domain comprises the Kaap Valley and Nelshoogte plutons with emplacement ages of 3223-3229 Ma (Kamo and Davis, 1994; Wang et al., 2020) and 3212-3236 Ma (Kamo and Davis, 1994; De Ronde and Kamo, 2000; Moyen et al., 2019; Wang et al., 2020), respectively and is located at the northwestern flank of the greenstone belt.

The late high-K granitoids (GGM) intruded the older TTG at high crustal levels as relatively thin sheets of large horizontal extent (e.g. (de Wit, 1998; Schoene et al., 2008) in a narrow time interval between 3106 Ma and 3109 Ma (Kamo and Davis, 1994; Poujol et

al., 2003). Interestingly, one GGM intrusion (Dalmein pluton), located in the Stolzburg domain, yields a U-Pb zircon age of 3216-3218 Ma (Kamo and Davis, 1994; Wang et al., 2020) that is clearly older than the main GGM intrusion event. The youngest GGM intrusion (Mpageni pluton) most probably represents a small volume of crustal melt that intruded at 2740 Ma (Kamo and Davis, 1994) and is most probably genetically related to the Nelspruit batholith.

3. Analytical techniques

To ensure sample homogeneity 5-10 kg of rock material was collected in the field. Sample rims were carefully removed and sample cores cut into 1-2 cm cubes using a diamond-coated saw. Samples cubes were crushed to chips using a Teflon-coated hydraulic press to minimise any metal alteration. For bulk rock geochemical analyses representative aliquots of 100-200 g of chips were finely powdered in an agate mill. Bulk rock Nd and Hf data were obtained on sample digests of 100 – 150 mg of sample powder.

Samarium-Nd, and Lu-Hf measurements were obtained on the Nu© Instruments multi-collector ICPMS at the University of Bern (Switzerland). Sm-Nd and Lu-Hf isotopes were separated from one single sintered rock digest following the procedure given in Kleinhanns et al. (2002). Measured values for JMC 475 Hf standard solution were 0.282164±16, 1.46733±5, and 1.88701±34 for $^{176}Hf/^{177}Hf$, $^{178}Hf/^{177}Hf$, and $^{180}Hf/^{177}Hf$, respectively. A Nd in-house standard solution gave values of 0.511070±20, 0.348414±12, and 0.236463±72 for $^{143}Nd/^{144}Nd$, $^{145}Nd/^{144}Nd$, and $^{150}Nd/^{144}Nd$, respectively. This in-house value corresponds to a value of 0.511860 for $^{143}Nd/^{144}Nd$ of La Jolla (Kleinhanns et al., 2002). Blank levels were consistently below 1ng and thus deemed negligible.

Argon measurements were performed on the MAP^{TM} 215-50B noble gas mass spectrometer at the University of Bern (Switzerland) using the incremental heating technique as described by Villa et al (2000). Samples were irradiated at the Risø research

reactor (DK) without Cd-shielding. For calculation of the respective J values MMhb-1 monitor was measured together with the samples.

4. Results

4.1. Bulk rock Sm-Nd and Lu-Hf isotope systematics

Samarium-Nd and Lu-Hf concentrations and their respective isotope ratios are given in Table 1. A Nd-evolution diagram (Fig. 2A) shows all samples age-corrected to their respective U-Pb zircon ages. The Stolzburg domain TTG display near-chondritic age-corrected ε(Nd)-values with a narrow range from +1.6 to –2.0 and thus, these TTG could be interpreted as products of relatively juvenile material. If all TTG are age-corrected to the age of the regional D2 event at 3.2 Ga, the low variability of ε(Nd)-values of 3.6 is further reduced to 3.0 ε–units (Fig. 2A), which may indicate that age correction beyond this event is not strictly valid (Moorbath et al., 1997). Kaap Valley domain TTG and the younger GGM suite were added to further constrain the crustal signature as these plutons are syn- to post-metamorphic with respect to the D2 event at ~3.2 Ga (Dziggel et al., 2002; Stevens et al., 2002; Kisters et al., 2003; Dziggel et al., 2005; Dziggel et al., 2006; Schoene and Bowring, 2010; Lana et al., 2011; Kröner et al., 2018). Zircon age-corrected ε(Nd)-values for the Kaap Valley domain TTG and GGM are sub-chondritic and only vary from –0.3 to –2.5. $T_{DM(Nd)}$ are up to 200 Ma older than their corresponding U-Pb zircon ages. TTG crust at the time of GGM intrusion had evolved to an average ε(Nd) value of –4 and as known from field relationships (de Wit, 1998) GGM additionally were fed by dykes cutting TTG crust. Thus, crustal contamination of GGM with (most probably) TTG-derived material or even derivation from it as seen in this data is a plausible mechanism to explain the observed isotopic relationship.

Zircon age-corrected ε(Hf)-values are mostly superchondritic for Stolzburg domain TTG and range between +5.1 and –-1.0 (Fig. 2B). This has been described for Nd in the literature (Schoene et al., 2009; Moyen et al., 2019) (not observed in our study), but the Hf isotopic composition is significantly more radiogenic. Importantly, the Stolzburg domain TTG, if age-corrected to the metamorphic event, would plot below the average DM-evolution line with less variable ε(Hf)-values of –0.9 to –6.2 and are thus in accordance with their Sm-Nd isotope characteristics. As a consequence of this agreement the same line of argumentation as used for Sm-Nd is valid for the Lu-Hf isotope system here and the question remains if age-correction of bulk rock isotopic data beyond the D2 event is valid. $T_{DM(Hf)}$ for Kaap Valley domain TTG and GGM correspond well to $T_{DM(Nd)}$ and are up to 300 Ma older compared to their respective U-Pb zircon ages. In addition, GGM span a narrow, slightly subchondritic, range of zircon age-corrected ε(Hf)-values from 0 to -2.4 (Fig. 2B). TTG crust, as most likely source, had evolved to ε(Hf)-values of around -5 at 3.1 Ga and thus, similar to the Sm-Nd isotopic system, the observed bulk rock Lu-Hf isotope systematics indicate crustal contamination or crustal derivation for the GGM.

4.2 Mineral Ar-Ar, Sm-Nd and Lu-Hf isotope signatures

The Stolzburg domain TTG yield initial ε(Hf) (this study, Table 1) and ε(Nd) (Schoene et al., 2009; Moyen et al., 2019) more radiogenic than the depleted mantle at their time of emplacement. To further understand the reason for this, we investigated various mineral phases of the Theespruit and Steynsdorp plutons for their Sm-Nd and Lu-Hf isotopes to test for possible later overprint during the D2 event and thus existing age discordance between different mineral phases (Table 2, Fig. 3 and 5). Thereby, titanite shows highly radiogenic Hf and Nd isotope signatures due to high Lu/Hf and Sm/Nd ratios. Additionally, it readily recrystallizes during metamorphism and deformation, and thus is a well suited candidate for

this kind of study. Apatite, amphibole, biotite and epidote, minerals known to react to metamorphic overprint similarly easily, were analysed to constrain the unradiogenic end of the array. To complement the data with an age determination that is unrelated to both studied isotope systems and is independent from zircon, we obtained Ar-Ar data from amphibole (Table 3, Fig. 4 and 6).

4.2.1 Steynsdorp pluton (sample 99/109)

In a Lu-Hf isochron plot (Fig. 3A), titanite and amphibole define an isochron age of 3202.7±8.9 Ma (MWSD of 2.0, model 1 (Ludwig, 2011)). This age is significantly younger than the corresponding U-Pb zircon ages between 3421 and 3553 Ma (Kamo and Davis, 1994; Kröner et al., 1996; Amelin et al., 2000; Poujol et al., 2003; Moyen et al., 2019; Laurent et al., 2020) strongly indicating a polyphase history for this pluton. The isochron age agrees within uncertainty with external age constraints for the regional D2 metamorphism at ~3.2 Ga adding further geological significance. Zircon Lu-Hf isotope data (Amelin et al., 2000) clearly plot below the regression line pointing to an older (still primary?) Hf isotope signature in these minerals indicating mineral age disequilibria in this pluton. Zircon grains recording an older still pristine Hf isotope signature within their (gneissic) granitoid hosts are described from the Ancient Gneiss Complex (Eswatini, Kröner et al. (2014)), Yilgarn craton (Australia) and Enderby Land in Antarctica (Hiess and Bennett, 2016). From the Steynsdorp pluton two WR-samples (99/109 and 99/122) have been investigated (Table 1) that yield similar $T_{DM(Hf)}$ of 3.35 Ga, respectively. Bulk rock mantle extraction ages are clearly younger than their corresponding U-Pb zircon ages and older than the Lu-Hf mineral isochron age. Both data-points, however, plot relatively close to or on the isochron regression line indicating near complete resetting of the Lu-Hf isotope system during the metamorphic overprint at 3.2 Ga. Thus, the $T_{DM(Hf)}$ of ~ 3.35 Ga are interpreted as mixing ages between a recalculated 'zircon-free' residual WR and zircon. In a

Sm-Nd isochron plot (Fig. 3B) titanite, apatite and amphibole yield an isochron age of 3204±15 Ma (MSWD of 2.0, model 1 (Ludwig, 2011)) that is within uncertainty equivalent to the Lu-Hf isochron age. The Sm-Nd mineral isochron age is well outside confidence limits of the reported corresponding U-Pb zircon ages between 3421Ma and 3553 Ma.

Argon measurements were performed on the supposedly single-generation, magmatic amphibole (Fig. 4, Table 3). Step ages are discordant and obtained ages are close to the Lu-Hf and Sm-Nd mineral isochron ages of 3202.7 ± 8.9 Ma and 3204 ± 15 Ma, respectively. A simple 'slow cooling' should produce very constant Cl/K and Ca/K ratios. Instead, the majority of step age variations are accompanied by variations of the Ca/K (and also Cl/K) compositional signature. The discordance of the age spectrum is evidence of internal mineral disequilibrium (Villa and Hanchar, 2017). In a chemical correlation diagram (e.g. (Villa et al., 1996) at least three reservoirs are needed. One required endmember Ca/K = 17 (steps 17-19) and is interpreted as amphibole Amp-1. A different phase with Ca/K = 14 is interpreted as amphibole Amp-2. Secondary phase(s) with Ca/K < 10 are probably not amphibole. The chemically homogeneous steps 17 to 19 define a concordant chemically homogenous subset with an average age of 3.24 Ga. As this age is resolvably older than the mineral isochron ages, Amp-1 may date an early phase of the metamorphic event, or more probably the presence of minor relicts of the magmatic amphibole. In contrast to the Ca-rich amphibole, the Cl-rich Amp-2 yields a significantly younger average age of 3.11 Ga on chemically homogeneous steps 4 to 8. The 3.11 Ga age can be related to the Cl-rich contact aureole of GGM intrusions. The steps carrying the Ar release of these compositionally defined end-members are separated by steps 9-16, which likely reflect partially overlapping temperature intervals, over which the amphibole generations degas. This mixes the isotopic signature of Amp-1 and Amp-2, resulting in intermediate Ca/K ratios and mixed ages producing a discordant age spectrum.

4.2.2 Theespruit pluton (sample 99/107)

Samarium-Nd and Lu-Hf isotope data were obtained on titanite, amphibole, epidote, biotite and apatite for this sample. Resulting age information is less clear compared to the Steynsdorp pluton (Fig. 5, Table 2). In a Lu-Hf isochron plot (Fig. 5A) the analysed minerals define a linear array that is controlled by the position of the respective titanite data points. A regression of titanite, amphibole and epidote analyses results in an errorchron age of 3340±17 Ma (MSWD of 4, model 3 (Ludwig, 2011)). Nevertheless, the errorchron age is resolvably younger than the corresponding U-Pb zircon ages of 3457-3470 Ma (Armstrong et al., 1990; Kamo and Davis, 1994; Poujol et al., 2003; Laurent et al., 2020) indicating a post-emplacement incomplete resetting of the Lu-Hf isotope system. Biotite separates define a subhorizontal linear array, which could be explained by sub-recent Lu gain. This is, however, not supported by their Lu and Hf concentrations as Lu concentrations are shown to be homogeneous while the Hf concentrations vary by one order of magnitude. Hf belongs to the group of HFS elements known to be immobile during fluid-controlled events and thus, the observed variation is interpreted to result from inclusions such as zircon or a mixture of inclusions. In addition, during hand-picking of the mineral separates a large amount of radiation haloes in biotite were observed and although we tried to eliminate such biotites during separation we cannot fully exclude the possibility of their existence in our measured separates. Zircon Lu-Hf isotope data (Zeh et al., 2009) plot slightly below the Lu-Hf errorchron regression line (Fig 5A) and shows similar $^{176}Hf/^{177}Hf$ ratios compared to two of the biotite separates. The separate with the highest Hf concentration however, shows slightly more radiogenic Hf contradicting this interpretation. Nevertheless, as no simple explanation for the biotites is possible at present, we can still argue for mineral disequilibria in the investigated sample due to the biotite results and more importantly, the resulting age is significantly younger than the corresponding U-Pb ages. In addition, the bulk rock analyses (99/107 and 99/121) diverge from the array defined by some of its minerals,

further pointing towards open-system behaviour with respect to the Lu-Hf isotope systematics.

A Sm-Nd isochron plot reveals similar isotope systematics as the Lu-Hf data. Titanite, amphibole, epidote and additionally apatite define a linear array, but with a much higher MSWD of 48 (model 3 (Ludwig, 2011); Fig. 5B). Albeit larger uncertainty and a small overlap in uncertainty with the reported 3437-3470 Ma U-Pb zircon ages, the resulting age of 3215±240 Ma is interpreted to be geologically relevant based on the significantly younger Lu-Hf age of this sample (Fig 5A) and its agreement with external age constraints for the D2 event. Biotite separates plot below the array defined by the other minerals. This is in contradiction to the conclusion drawn from their Lu-Hf systematics as zircon inclusions should result in data-points lying above the defined array. The unradiogenic biotite could be explained with monazite inclusion due to its low $^{147}Sm/^{144}Nd$ ratio. This argument is, however, not valid for the other biotite separate that shows a high $^{147}Sm/^{144}Nd$ ratio. Again, the biotite data is not easy to explain, but nevertheless they indicate internal mineral disequilibria. More importantly, both WRs lie slightly below the defined array further emphasising internal heterogeneities. Thus, both the Lu-Hf and Sm-Nd systematics appear to have acted as open systems during a post-emplacement overprint.

Ar-Ar results for the pluton display similar degassing behaviour and similar resulting age spectra for both analysed amphibole size fractions (Fig. 6, Table 3) that display in addition a similar pattern compared to the Steynsdorp pluton. Step ages are discordant and obtained ages are significantly lower than the corresponding U-Pb zircon ages. The majority of step ages, however, are similar to the externally derived age constraint for the *ca.* 3.2 Ga D2 metamorphic overprint (large fraction: steps 4-6, 11-13, 19, 20; small fraction: 3-5, 18-20). The intermediate steps (mostly degassed between 1000°C and 1240°C) yield more variable step ages that can be viewed as mixing between two heterochemical amphibole generations: a Ca-rich generation formed during the 3.20 Ga

metamorphic event and a Cl-rich generation related to the ca. 3.1 Ga GGM intrusion event. A plot of Cl/K vs. Ca/K ratios indicate a mixing between at least three reservoirs, although Ca/K is much less variable than Cl/K. One possible endmember is given at low Cl/K (step 16) and subsequently, a diversion towards higher Cl/K ratios together with more variable Ca/K ratios is observed. Comparison of these ratios with their respective step ages reveals a chemical correlation that is weakly negative for Cl/K and weakly positive with respect to Ca/K. Hence, age information derived from zircon and amphibole are complementary, indicating a polyphase history for this pluton.

5. Discussion

5.1 Geochronology of the Stolzburg domain TTG

Both TTG intrusions (Theespruit and Steynsdorp pluton) investigated on a mineral basis show internal age disequilibria with respect to their Sm-Nd and Lu-Hf isotope systematics. These disequilibria are interpreted to result from the regional D2 event at 3.2 Ga and to a lesser degree also the GGM intrusion event at 3.1 Ga. Presented age data provide evidence for a decoupling of zircon and 'zircon-free' bulk rock. This is further emphasised in a comparison of all available geochronological data (Fig. 7) where both TTG plutons studied in detail show a similar pattern. Published U-Pb zircon ages for the Theespruit and Steynsdorp plutons are 3437-3470 Ma and 3421-3553 Ma, respectively (Kamo and Davis, 1994; Amelin et al., 2000; Poujol et al., 2003; Schoene et al., 2008; Zeh et al., 2009; Moyen et al., 2019; Laurent et al., 2020). These most probably encompass the timing of emplacement whereby the range of zircon U-Pb ages especially seen in the Steynsdorp pluton spans well over a 100 Ma. Similar observations for zircons in old crustal rocks from Pilbara, Slave and Kaapvaal cratons were interpreted as multiple zircon growth or ancient Pb loss (Amelin et al., 2000; Kröner et al., 2014; Laurent et al., 2020). Corresponding zircon $T_{DM(Hf)}$ of both plutons yield similar ages of 3.48±0.07 Ga and 3.53±0.08 Ga,

respectively (Lu-Hf zircon data from Zeh et al. (2009), Amelin et al. (2000)). Additionally, another pluton of this domain, the Stolzburg pluton, shows a similar relationship with U-Pb and $T_{DM(Hf)}$ ages of 3431- 3460 Ma and 3.48±0.06 Ga, respectively.

The similarity of U-Pb and $T_{DM(Hf)}$ zircon ages argues against a long crustal residence time or assimilation of pre-existing crust before emplacement of the Stolzburg domain TTG. Recently, Laurent et al. (2020) interpreted the Stolzburg domain trondhjemitic TTG to be produced entirely intracrustal out of a tonalitic parental magma, which in turn was the result of lower crustal melting of mafic precursors. These authors further state that this whole process happened in short timescales of ~10 Ma that could explain the aforementioned similarity of zircon U-Pb and $T_{DM(Hf)}$ ages in Stolzburg domain TTG. In combination with the paucity of inherited zircons (Moyen et al., 2019) this strongly argues for melt extraction at that time and does not hint towards sampling of an older felsic lithospheric reservoir as stated for example by Kröner et al. (2014) and Schoene et al. (2009).

Regarding the Sm-Nd and Lu-Hf isotope systems, the regional D2 metamorphic event at 3.2 Ga led to an almost complete reset in the Steynsdorp pluton and a partial reset of the Theespruit pluton. Mineral isochron ages correspond to the age of the D2 event and are significantly younger than the corresponding U-Pb zircon ages. Amphibole further shows younger Ar-Ar ages that also correspond to the regional metamorphic D2 and to the 3.1 Ga GGM intrusion event. Further evidence for post-emplacement activity in Stolzburg terrain TTG is given by ca. 3.2 Ga U-Pb ages of rutile, apatite, titanite and to a lesser degree zircon (Kamo and Davis, 1994; Schoene et al., 2008) and even some younger apatite ages corresponding to the 3.1 Ga GGM intrusion event (Schoene et al., 2008). As a consequence of this recorded age spectra, bulk rock T_{DM} data yield unclear results, since it contains pristine (e.g. zircon) and reset (e.g. titanite, amphibole, apatite, epidote) mineral phases. Mantle extraction ages calculated from Steynsdorp WR data yield similar $T_{DM(Hf)}$ of 3.35

Ga whereas the analogous $T_{DM(Nd)}$ yield highly variable ages of 3.33 Ga and 3.47 Ga, respectively. In case of the Theespruit pluton determined bulk rock mantle extraction ages also yield unclear results with $T_{DM(Nd)}$ of 3.49 and 3.56 Ga and $T_{DM(Hf)}$ of 3.37 and 3.54 Ga. Thus, our data indicate open-system behaviour of the Sm-Nd and Lu-Hf isotope systems during the amphibolite-facies metamorphism, which disturbed the bulk rock parent/daughters ratio of these rocks. This has also been described for other similarly old crustal rocks previously (Hammerli et al., 2014; Kröner et al., 2014; Pandey et al., 2019; Fisher et al., 2020). A lowering of the parent/daughter ratio during metamorphism that occurred significantly later than emplacement would lead to an erroneous extrapolation of the evolution line in Sm-Nd and Lu-Hf space giving too young mantle extraction ages and too high initial values (Arndt and Goldstein, 1987; Kröner et al., 2014; Vervoort and Kemp, 2016). An increase would lead to the opposite result. The issue of changed trace element concentrations (and thus ultimately changed parent/daughter ratios) has been discussed in a number of studies investigating early Archean rocks (e.g (Moorbath et al., 1997; Schoene et al., 2009; Schneider et al., 2018; Moyen et al., 2019; Pandey et al., 2019). Concentration changes in our studied samples obviously occur at the percent level that are not easily detectable by "classical" spidergrams (due to their use of log compression: see, e.g., Haskin (1990)) without applying detailed isotope geochemical investigations. The trace element pattern of the BML TTGs are similar for all different age groups (Kleinhanns et al., 2003) and the older Stolzburg domain TTG do not show any obvious signs for a later overprint. Based on these observations and results it is proposed here that bulk rock ε(Hf) and ε(Nd) values for the >3.45 Ga TTGs of the Stolzburg domain calculated further back in time than the D2 event at 3.2 Ga are found to be incorrect / questionable when critically assessed in detail. Zircon ε(Hf) seems to be more robust as visible in the good and plausible correlation with corresponding U-Pb isotope data, but can be de-coupled from the bulk rock isotopic

signature as previously shown for strongly migmatitic samples derived from the Ancient Gneiss complex in Eswatini (Kröner et al., 2014).

5.2 Re-investigated petrogenesis of BML granitoids

5.2.1 Stolzburg domain TTG (pre-D2 granitoids)

The TTG of the Stolzburg domain are interpreted as a single crustal entity (Schoene et al., 2009; Moyen et al., 2019) within the Barberton Mountain Land. This interpretation is of course still valid since these plutons all show emplacement ages older than 3.45 Ga and thus are distinct in comparison to the younger neighbouring plutonic domains. Their petrogenetic interpretation, however, has to be re-investigated in the light of the previously presented findings.

The observed range of zircon age-corrected bulk rock ε(Nd) and ε(Hf) values for these TTGs is relatively large (e.g. this study, Schoene et al. (2009); Moyen et al. (2019)) with values between -4 to 5 and -2 to 5, respectively. Schoene et al. (2009) interpreted (only based on Nd isotopes) these signatures to reflect the admixture of older crust to juvenile mantle melts in various amounts. This is in contradiction with the major and trace element characteristics that indicate derivation from a "primitive-mantle"-like reservoir (Moyen et al 2019). Assimilation of pre-existing felsic crust is further considered unlikely as these plutons lack abundant inherited zircon (Moyen et al., 2019) and zircon U-Pb-Hf data indicate melt extraction and zircon crystallisation to be closely related in time (section 5.1.). The documented open-system behaviour of the Sm-Nd and Lu-Hf isotope systems offers another possibility to explain the observed high variation of bulk rock Nd and Hf isotope signatures. Age corrected bulk rock ε(Nd) and ε(Hf) values at the time of the D2 event range from -0.9 to -6.2 and -1.3 to -4.3 for the Stolzburg domain TTGs. These values are well below the depleted mantle at that time and thus an early more evolved reservoir is not

required to explain the observed Sm-Nd and Lu-Hf isotopic data. Modelling the $^{176}Lu/^{177}Hf$ ratio forward in time to fit the evolutionary trend of the samples from the initial $^{176}Hf/^{177}Hf$ value of the zircons (Amelin et al., 2000; Zeh et al., 2009) to the observed bulk rock Hf isotopic composition at the time of D2 gives values between 0.014 and 0.038. These ratios are unreasonably high as TTGs are characterised by low Lu/Hf ratios and steep REE patterns generally explained by residual garnet. André et al. (2019), however, recently offered another interesting possibility explaining lowered Lu/Hf ratios by alteration (and silicification) of the mafic precursor rocks based on the observed correlation of Lu/Hf with the $\delta^{30}Si$ isotope signatures. Nevertheless, as the modelled Lu/Hf ratios are almost as high as the value for the depleted mantle and are therefore considered unlikely for a partial melt with the higher incompatibility of Hf over Lu (and even more so if the partial melt derived from a pre-existing mafic crust). Thus, the relationship between the zircon grains and their host TTG is not simple and not easily explainable. Nevertheless, the presented data clearly shows that the Stolzburg domain TTGs underwent significant (isotope) geochemical modification during their burial to lower crustal depth ca. 250 Ma after their formation.

5.2.2 Kaap Valley TTG (syn-D2 granitoids)

Kaap Valley TTGs were emplaced contemporaneously with the D2 event. Nd-Hf isotopic signatures for the Kaap Valley TTGs are in a similar range with Stolzburg domain TTG at the time of D2 (Fig. 2) pointing towards evolution out of a pre-existing reservoir with a more evolved isotope signature as already proposed by Zeh et al. (2009) based zircon Lu-Hf isotopic data. Additionally, minor inherited zircon is present in the Nelshoogte pluton with U-Pb ages of 3477 Ma that corresponds to the emplacement age of the Stolzburg domain TTG (Guitreau et al., 2012) supporting this interpretation.

5.2.3 GGM intrusions (post-D2 granitoids)

The last major magmatic episode is re-presented by the intrusion of the extensive 3.1 Ga post-D2 GGM. Their bulk rock Hf-Nd isotope signatures support previous interpretations as lower crustal melts as all T_{DM} are significantly older than their respective U-Pb zircon ages and point towards intracrustal melting. In line with this interpretation a number of inherited zircon xenocrysts are reported (Kamo and Davis, 1994; Zeh et al., 2009).

The Mpageni pluton (sample 99/111) represents the only known small scale intrusion north of the BML with a U-Pb zircon age as young as 2.74 Ga and thus has not been discussed in detail within this study. Nevertheless, one interesting conclusion can be drawn from its results in that both investigated isotope systems give mantle extraction ages of ~3.1 Ga, compared with the younger U-Pb zircon age of 2.74 Ga. As this pluton is located in the large Nelspruit batholith north of BML that was dated with U-Pb zircon to 3.1 Ga, no detectable fractionation seems to have occurred between these two systems during intracrustal fractionation (e.g. anatectic processes).

6. Summary

Pre-D2 TTG of the Stolzburg domain probably were derived from a 'primitive-mantle'-like reservoir and do not show evidence for the existence of an older more evolved mantle reservoir. Zircon U-Pb-Hf isotope signatures show that melt extraction and zircon crystallisation were closely related in time. The petrochronological evidence provided unanimously by the Sm-Nd, Lu-Hf and K-Ar systems demonstrates that the constituent minerals were affected by the regional metamorphic D2 event ca. 250 Ma after their formation and record isotopic disequilibrium. Therefore the whole-rock systems are also in isotopic disequilibrium with the primary igneous zircon, and the extrapolation of Hf and Nd signatures based on zircon is geologically insignificant. The resetting of the bulk rock Sm-Nd and Lu-Hf isotope systems led to the isotopic de-coupling of zircon from the zircon-free residual whole rock. Samples with high apparent initials indicate a lowering of the

parent/daughter ratio and calculated mantle extraction ages of these samples are to be interpreted as minimum ages for the generation of the felsic TTG crust of Barberton Mountain Land. Thus, the minimum estimate for primary felsic crustal generation in this region is ~ 3.5 Ga in accordance with reported U-Pb zircon ages from BML. In case of the syn- and post-D2 granitoids all investigated isotope constraints allow for crustal contamination and/or melting of lower crust. Consequently the 3.1 Ga intrusion event led to a barren lower crust and hence, stabilisation of the Kaapvaal craton in that area.

Acknowledgements

Constructive reviews by J. Elis Hoffmann and Jörn-Frederik Wotzlaw that enhanced the quality of this study are greatly acknowledged. We would like to thank Chris Hawkesworth, who gave highly constructive comments on an earlier version of this manuscript that helped a lot in improving this study. ICK thanks Annett Buettner greatly for the introduction to the Ar isotope world and analytical support. Ronny Schoenberg kindly provided samples and the electronic map in Figure 1. Isotope Geology Research at the University of Bern is funded by the Swiss National Science Foundation (Grant-No. 20-61933.00).

Declaration of interests

☒ The authors declare that they have no known competing financial interests or personal relationships that could have appeared to influence the work reported in this paper.

References

Amelin, Y., Lee, D.C., Halliday, A.N., 2000. Early-middle Archaean crustal evolution deduced from Lu-Hf and U-Pb isotopic studies of single zircon grains. Geochimica Et Cosmochimica Acta, 64(24): 4205-4225.

André, L., Abraham, K., Hofmann, A., Monin, L., Kleinhanns, I.C., Foley, S., 2019. Early continental crust generated by reworking of basalts variably silicified by seawater. Nature Geoscience, 12(9): 769-773.

Anhaeusser, C.R., 2010. Magmatic and structural characteristics of the ca. 3440 Ma Theespruit pluton, Barberton Mountain Land, South Africa. American Journal of Science, 310(9): 1136.

Armstrong, R.A., Compston, W., de Wit, M.J., Williams, I.S., 1990. The stratigraphy of the 3.5-3.2 Ga Barberton Greenstone Belt revisited: A single zircon ion microprobe study. Earth and Planetary Science Letters, 101(1): 90-106.

Arndt, N.T., Goldstein, S.L., 1987. Use and abuse of crust-formation ages. Geology, 15(10): 893-895.

Bennett, V.C., Nutman, A.P., McCulloch, M.T., 1993. Nd-isotopic evidence for transient, higjly depleted mantle reservoirs in the early hsitory of the earth. Earth and Planetary Science Letters, 119(3): 299-317.

Blichert-Toft, J., Frei, R., 2001. Complex Sm-Nd and Lu-Hf isotope systematics in metamorphic garnets from the Isua supracrustal belt, West Greenland. Geochimica Et Cosmochimica Acta, 65(18): 3177-3189.

Bouvier, A., Vervoort, J.D., Patchett, P.J., 2008. The Lu-Hf and Sm-Nd isotopic composition of CHUR: Constraints from unequilibrated chondrites and implications for the bulk composition of terrestrial planets. Earth and Planetary Science Letters, 273(1-2): 48-57.

Bowring, S.A., Housh, T., 1995. The Early earth evolution. Science, 269(5230): 1535-1540.

Bowring, S.A., Williams, I.S., 1999. Priscoan (4.00-4.03 Ga) orthogneisses from northwestern Canada. Contributions to Mineralogy and Petrology, 134(1): 3-16.

Caro, G., Bourdon, B., Birck, J.L., Moorbath, S., 2006. High-precision Nd-142/Nd-144 measurements in terrestrial rocks: Constraints on the early differentiation of the Earth's mantle. Geochimica Et Cosmochimica Acta, 70(1): 164-191.

Cherniak, D.J., Watson, E.B., 2003. Diffusion in zircon. In: Hanchar, J.M., Hoskin, P.W.O. (Eds.), Zircon. Reviews in Mineralogy & Geochemistry, pp. 113-143.

De Ronde, C.E.J., Kamo, S.L., 2000. An Archaean arc-arc collisional event: a short-lived (ca 3 Myr) episode, Weltevreden area, Barberton greenstone belt, South Africa. Journal of African Earth Sciences, 30(2): 219-248.

de Wit, M.J., 1998. On Archean granites, greenstones, cratons and tectonics: does the evidence demand a verdict? Precambrian Research, 91(1-2): 181-226.

Diener, J.F.A., Stevens, G., Kisters, A.F.M., Poujol, M., 2005. Metamorphism and exhumation of the basal parts of the Barberton greenstone belt, South Africa:

Constraining the rates of Mesoarchaean tectonism. Precambrian Research, 143(1-4): 87-112.

Dziggel, A., Stevens, G., Poujol, M., Anhaeusser, C.R., Armstrong, R.A., 2002. Metamorphism of the granite-greenstone terrane south of the Barberton greenstone belt, South Africa: an insight into the tectono-thermal evolution of the 'lower' portions of the Onverwacht Group. Precambrian Research, 114(3-4): 221-247.

Dziggel, A., Armstrong, R.A., Stevens, G., Nasdala, L., 2005. Growth of zircon and titanite during metamorphism in the granitoid-gneiss terrane south of the Barberton greenstone belt, South Africa. Mineralogical Magazine, 69(6): 1019-1036.

Dziggel, A., Knipfer, S., Kisters, A.F.M., Meyer, F.M., 2006. P-T and structural evolution during exhumation of high-T, medium-P basement rocks in the Barberton Mountain Land, South Africa. Journal of Metamorphic Geology, 24(7): 535-551.

Fisher, C.M., Bauer, A.M., Vervoort, J.D., 2020. Disturbances in the Sm–Nd isotope system of the Acasta Gneiss Complex—Implications for the Nd isotope record of the early Earth. Earth and Planetary Science Letters, 530: 115900.

Guitreau, M., Blichert-Toft, J., Martin, H., Mojzsis, S.J., Albarède, F., 2012. Hafnium isotope evidence from Archean granitic rocks for deep-mantle origin of continental crust. Earth and Planetary Science Letters, 337-338: 211-223.

Hammerli, J., Kemp, A.I.S., Spandler, C., 2014. Neodymium isotope equilibration during crustal metamorphism revealed by in situ microanalysis of REE-rich accessory minerals. Earth and Planetary Science Letters, 392: 133-142.

Haskin, L.A., 1990. PREEconceptions pREEvent pREEcise pREEdictions. Geochimica et Cosmochimica Acta, 54(9): 2353-2361.

Hawkesworth, C.J., Kemp, A.I.S., 2006. Using hafnium and oxygen isotopes in zircons to unravel the record of crustal evolution. Chemical Geology, 226(3-4): 144-162.

Hiess, J., Bennett, V.C., 2016. Chondritic Lu/Hf in the early crust–mantle system as recorded by zircon populations from the oldest Eoarchean rocks of Yilgarn Craton, West Australia and Enderby Land, Antarctica. Chemical Geology, 427: 125-143.

Hoffmann, J.E., Munker, C., Polat, A., Konig, S., Mezger, K., Rosing, M.T., 2010. Highly depleted Hadean mantle reservoirs in the sources of early Archean arc-like rocks, Isua supracrustal belt, southern West Greenland. Geochimica Et Cosmochimica Acta, 74(24): 7236-7260.

Hoffmann, J.E., Munker, C., Polat, A., Rosing, M.T., Schulz, T., 2011. The origin of decoupled Hf-Nd isotope compositions in Eoarchean rocks from southern West Greenland. Geochimica Et Cosmochimica Acta, 75(21): 6610-6628.

Hofmann, A.W., 1988. Chemical differentiation of the Earth - The relationship between mantle, continental-crust, and oceanic-crust. Earth and Planetary Science Letters, 90(3): 297-314.

Huang, H., Niu, Y., Teng, F.-Z., Wang, S.-J., 2019. Discrepancy between bulk-rock and zircon Hf isotopes accompanying Nd-Hf isotope decoupling. Geochimica et Cosmochimica Acta, 259: 17-36.

Kamber, B.S., Moorbath, S., Whitehouse, M.J., 1998. Extreme Nd-isotope heterogeneity in the early Archaean - fact or fiction? Case histories from northern Canada and west Greenland - Reply. Chemical Geology, 148(3-4): 219-224.

Kamber, B.S., Collerson, K.D., 2000. Role of 'hidden' deeply subducted slabs in mantle depletion. Chemical Geology, 166(3-4): 241-254.

Kamo, S.L., Davis, D.W., 1994. Reassessment of Archean crustal development in the Barberton Mountain Land, South-Africa based on U-Pb dating. Tectonics, 13(1): 167-192.

Kemp, A.I.S., Hawkesworth, C.J., Paterson, B.A., Kinny, P.D., 2006. Episodic growth of the Gondwana supercontinent from hafnium and oxygen isotopes in zircon. Nature, 439(7076): 580-583.

Kemp, A.I.S., Wilde, S.A., Hawkesworth, C.J., Coath, C.D., Nemchin, A., Pidgeon, R.T., Vervoort, J.D., DuFrane, S.A., 2010. Hadean crustal evolution revisited: New constraints from Pb-Hf isotope systematics of the Jack Hills zircons. Earth and Planetary Science Letters, 296(1-2): 45-56.

Kisters, A.F.M., Stevens, G., Dziggel, A., Armstrong, R.A., 2003. Extensional detachment faulting and core-complex formation in the southern Barberton granite-greenstone terrain, South Africa: evidence for a 3.2 Ga orogenic collapse. Precambrian Research, 127(4): 355-378.

Kisters, A.F.M., Belcher, R.W., Poujol, M., Dziggel, A., 2010. Continental growth and convergence-related arc plutonism in the Mesoarchaean: Evidence from the Barberton granitoid-greenstone terrain, South Africa. Precambrian Research, 178(1-4): 15-26.

Kleinhanns, I.C., Kreissig, K., Kamber, B.S., Meisel, T., Nagler, T.F., Kramers, J.D., 2002. Combined chemical separation of Lu, Hf, Sm, Nd, and REEs from a single rock

digest: Precise and accurate isotope Determinations of Lu-Hf and Sm-Nd using multicollector-ICPMS. Analytical Chemistry, 74(1): 67-73.

Kleinhanns, I.C., Kramers, J.D., Kamber, B.S., 2003. Importance of water for Archaean granitoid petrology: a comparative study of TTG and potassic granitoids from Barberton Mountain Land, South Africa. Contributions to Mineralogy and Petrology, 145(3): 377-389.

Kröner, A., Hegner, E., Wendt, J.I., Byerly, G.R., 1996. The oldest part of the Barberton granitoid-greenstone terrain, South Africa: evidence for crust formation between 3.5 and 3.7 Ga. Precambrian Research, 78(1): 105-124.

Kröner, A., Hoffmann, J.E., Xie, H., Münker, C., Hegner, E., Wan, Y., Hofmann, A., Liu, D., Yang, J., 2014. Generation of early Archaean grey gneisses through melting of older crust in the eastern Kaapvaal craton, southern Africa. Precambrian Research, 255: 823-846.

Kröner, A. et al., 2018. High-temperature metamorphism and crustal melting at ca. 3.2 Ga in the eastern Kaapvaal craton, southern Africa. Precambrian Research, 317: 101-116.

Lana, C., Buick, I., Stevens, G., Rossouw, R., De Wet, W., 2011. 3230-3200 Ma post-orogenic extension and mid-crustal magmatism along the southeastern margin of the Barberton Greenstone Belt, South Africa. Journal of Structural Geology, 33(5): 844-858.

Laurent, O., Björnsen, J., Wotzlaw, J.-F., Bretscher, S., Pimenta Silva, M., Moyen, J.-F., Ulmer, P., Bachmann, O., 2020. Earth's earliest granitoids are crystal-rich magma reservoirs tapped by silicic eruptions. Nature Geoscience, 13(2): 163-169.

Lowe, D.R., 1999. Geologic evolution of the Barberton Greenstone Belt and vicinity. In: Lowe, D.R., Byerly, G.R. (Eds.), Geologic Evolution of the Barberton Greenstone Belt, South Africa. Geological Society of America, pp. 0.

Ludwig, K.R., 2011. A geochronological toolkit for microsoft Excel. Berkeley Geochronology Centre Special Publications, Version 4.1.

Macdonald, R., Hawkesworth, C.J., Heath, E., 2000. The Lesser Antilles volcanic chain: a study in are magmatism. Earth-Science Reviews, 49(1-4): 1-76.

Mezger, K., Krogstad, E.J., 1997. Interpretation of discordant U-Pb zircon ages: An evaluation. Journal of Metamorphic Geology, 15(1): 127-140.

Moorbath, S., Whitehouse, M.J., Kamber, B.S., 1997. Extreme Nd-isotope heterogeneity in the early Archaean - Fact or fiction? Case histories from northern Canada and West Greenland. Chemical Geology, 135(3-4): 213-231.

Moyen, J.-F., Stevens, G., Kisters, A.F.M., Belcher, R.W., Lemirre, B., 2019. Chapter 25 - TTG Plutons of the Barberton Granitoid-Greenstone Terrain, South Africa. In: Van Kranendonk, M.J., Bennett, V.C., Hoffmann, J.E. (Eds.), Earth's Oldest Rocks (Second Edition). Elsevier, pp. 615-653.

Pandey, O.P., Mezger, K., Ranjan, S., Upadhyay, D., Villa, I.M., Nägler, T.F., Vollstaedt, H., 2019. Genesis of the Singhbhum Craton, eastern India; implications for Archean crust-mantle evolution of the Earth. Chemical Geology, 512: 85-106.

Payne, J.L., McInerney, D.J., Barovich, K.M., Kirkland, C.L., Pearson, N.J., Hand, M., 2016. Strengths and limitations of zircon Lu-Hf and O isotopes in modelling crustal growth. Lithos, 248-251: 175-192.

Poujol, M., Robb, L.J., Anhaeusser, C.R., Gericke, B., 2003. A review of the geochronological constraints on the evolution of the Kaapvaal Craton, South Africa. Precambrian Research, 127(1): 181-213.

Rubatto, D., 2017. Zircon: The Metamorphic Mineral. Reviews in Mineralogy and Geochemistry, 83(1): 261-295.

Sanchez-Garrido, C., Stevens, G., Armstrong, R.A., Moyen, J.F., Martin, H., Doucelance, R., 2011. Diversity in Earth's early felsic crust: Paleoarchean peraluminous granites of the Barberton Greenstone Belt. Geology, 39(10): 963-966.

Schneider, K.P., Hoffmann, J.E., Boyet, M., Munker, C., Kroner, A., 2018. Coexistence of enriched and modern-like Nd-142 signatures in Archean igneous rocks of the eastern Kaapvaal Craton, southern Africa. Earth and Planetary Science Letters, 487: 54-66.

Schoene, B., de Wit, M.J., Bowring, S.A., 2008. Mesoarchean assembly and stabilization of the eastern Kaapvaal craton: A structural-thermochronological perspective. Tectonics, 27(5).

Schoene, B., Dudas, F.O.L., Bowring, S.A., de Wit, M., 2009. Sm-Nd isotopic mapping of lithospheric growth and stabilization in the eastern Kaapvaal craton. Terra Nova, 21(3): 219-228.

Schoene, B., Bowring, S.A., 2010. Rates and mechanisms of Mesoarchean magmatic arc construction, eastern Kaapvaal craton, Swaziland. Geological Society of America Bulletin, 122(3-4): 408-429.

Stevens, G., Droop, G.T.R., Armstrong, R.A., Anhaeusser, C.R., 2002. Amphibolite facies metamorphism in the Schapenburg Schist Belt: A record of the mid-crustal response to-3.23 Ga terrane accretion in the Barberton greenstone belt. South African Journal of Geology, 105(3): 271-284.

Szilas, K., Hoffmann, J.E., Schulz, T., Hansmeier, C., Polat, A., Viehmann, S., Kasper, H.U., Munker, C., 2016. Combined bulk-rock Hf- and Nd-isotope compositions of Mesoarchaean metavolcanic rocks from the Ivisaartoq Supracrustal Belt, SW Greenland: Deviations from the mantle array caused by crustal recycling. Chemie Der Erde-Geochemistry, 76(4): 543-554.

Tang, M., Wang, X.-L., Shu, X.-J., Wang, D., Yang, T., Gopon, P., 2014. Hafnium isotopic heterogeneity in zircons from granitic rocks: Geochemical evaluation and modeling of "zircon effect" in crustal anatexis. Earth and Planetary Science Letters, 389: 188-199.

Vervoort, J.D., Patchett, P.J., Gehrels, G.E., Nutman, A.P., 1996. Constraints on early Earth differentiation from hafnium and neodymium isotopes. Nature, 379(6566): 624-627.

Vervoort, J.D., Kemp, A.I.S., 2016. Clarifying the zircon Hf isotope record of crust-mantle evolution. Chemical Geology, 425: 65-75.

Villa, I.M., Grobéty, B., Kelley, S.P., Trigila, R., Wieler, R., 1996. Assessing Ar transport paths and mechanisms in the McClure Mountains hornblende. Contributions to Mineralogy and Petrology, 126(1): 67-80.

Villa, I.M., Hermann, J., Muntener, O., Trommsdorff, V., 2000. Ar-39-Ar-40 dating of multiply zoned amphibole generations (Malenco, Italian Alps). Contributions to Mineralogy and Petrology, 140(3): 363-381.

Villa, I.M., Hanchar, J.M., 2017. Age discordance and mineralogy. American Mineralogist, 102(12): 2422-2439.

Wang, H., Yang, J.-H., Kröner, A., Zhu, Y.-S., Wei, Q.-D., Li, R., Xu, L., 2020. Extensive magmatism and metamorphism at ca. 3.2 Ga in the eastern Kaapvaal Craton. Precambrian Research, 351: 105952.

Whitehouse, M.J., Nagler, T.F., Moorbath, S., Kramers, J.D., Kamber, B.S., Frei, R., 2001. Priscoan (4.00-4.03 Ga) orthogneisses from northwestern Canada - by Samuel A. Bowring and Ian S. Williams: discussion. Contributions to Mineralogy and Petrology, 141(2): 248-250.

Zeh, A., Gerdes, A., Barton, J.M., 2009. Archean Accretion and Crustal Evolution of the Kalahari Craton-the Zircon Age and Hf Isotope Record of Granitic Rocks from Barberton/Swaziland to the Francistown Arc. Journal of Petrology, 50(5): 933-966.

Figure 1: Simplified geological map of the Barberton Mountain Land (Kaapvaal Craton, South Africa) showing the sampling sites and loca"ons of the Theespruit and Steynsdorp plutons, respec"vely. GPS coordinates for sampling sites are given in Table 1.

Figure 2: Bulk rock Sm-Nd and Lu-Hf isotope systematics of GGM and TTG; GGM indicate involvement of an older crustal component. TTG point towards inheritance of older zircons and/or open-system behavior during the 3.2 Ga event; see text for further discussion; DM lines were calculated backwards in time using the parameters given in Table1. **(A)** Nd evolution diagram with age-correction to their respective zircon U-Pb ages; **(B)** Hf evolution diagram with age-correction to their respective zircon U-Pb ages

Figure 3: Lu-Hf **(A)** and Sm-Nd **(B)** isochron calculations (Isoplot version 4.15, Ludwig 2011) for sample 99/109 (Steynsdorp pluton). Regression ages for both systems agree within uncertainty with the 3.2 Ga D2 event and are distinctly younger than reported U/Pb zircon age of 3421-3352 Ma (Table 1). WR samples (99/109 and 99/122) are not included in the regression, because of suspected incomplete resetting.

Figure 4: Amphibole ^{40}Ar-^{39}Ar results for sample 99/109 (Steynsdorp pluton). Steps 1, 2, 3 and 20, which can be identified as minor contaminant phases due to their low Ca, low step ages and high uncertainty, respectively, are not further considered for interpretation. **(A)** Age spectrum. Externally derived age constraints are shown as grey bars. All step ages clearly plot below their corresponding U/Pb zircon ages of 3440-3470 Ma (Table 1) and give ages that scatter between the age of metamorphic overprint and GGM intrusion event. **(B)** Age vs. Ca/K diagram. The positive correlation may be interpreted as mixing between one (or more) high-Ca/K regional metamorphic amphibole(s) and one (or more) low-Ca/K contact metamorphic amphibole(s).

Figure 5: Lu-Hf **(A)** and Sm-Nd **(B)** isochron calculations (Isoplot version 4.15, Ludwig 2011) for sample 99/107 (Theespruit pluton). Regression ages for both systems agree within uncertainty with the 3.2 Ga D2 event and are distinctly younger from reported U/Pb zircon ages of 3440-3470 Ma (Kamo & Davies 1994). WR samples (99/107 and 99/121) are not included in the regression, because of suspected incomplete resetting.

Figure 6: **^{40}Ar-^{39}Ar results for sample 99/107 (Theespruit pluton). Amphiboles were sieved in two size fractions and analysed separately. For ease of comparison both fractions are plotted together. Steps 1 and 2 of both aliquots have a very low Ca/K ratio, and are therefore identified as secondary phases, not as amphibole and hence not**

considered for interpretation. (A) **Age spectrum. Externally derived age constraints are shown as grey bars. Relevant step ages clearly plot below their corresponding U/Pb zircon age (Kamo and Davis, 1994) and give ages that scatter between the age of metamorphic overprint and GGM intrusion event.** (B) **Chemical correlation diagram. Cl/K ratios scatter to a much higher degree than Ca/K ratios. Spread of steps indicate mixing with at least three reservoirs, with younger ages at higher Cl/K ratios. Step 16 is a vertex of the polygon enclosing the other heating steps, and is therefore a likely end-member of the ternary mixture.** (C) **Plot of step age vs. Cl/K ratio . Younger step ages show higher Cl/K ratios.** (D) **Plot of step age vs. Ca/K ratio showing a weak positive correlation between Ca/K and step ages**

Figure 7: Schematic plot of available age data for **(A)** Steynsdorp pluton and **(B)** Theespruit pluton. No significance on y-axis. Zircon age information relates to the primary intrusion event whereas other mineral age information can be related to either the regional D2 metamorphic or the GGM intrusion event and thus records later overprint. Consequently, bulk rock age information gives erroneous ages that cannot be related to any event based on heterogenous chronological information saved in different mineral phases and testify to the polyphase history of both investigated plutons. See text for further discussion. Literature data: U-Pb zircon data see Table 1 ; zircon Hf isotope data from Amelin et al 2000, Zeh et al 2009.

Table 1: WR Lu-Hf and Sm-Nd isotope data on the investigated granitoids of Barberton Mountain Land

sample ID	pluton	GPS coordinates	zircon age[a] [Ma]	Lu [µg/g]	Hf [µg/g]	$^{176}Lu/^{177}Hf$	$^{176}Hf/^{177}Hf$	± 2 S.E.	eps (0)	T_{DM}[b] [Ga]	eps (zircon age)	eps (D2; 3200 Ma)	Sm [µg/g]	Nd [µg/g]	$^{147}Sm/^{144}Nd$	$^{143}Nd/^{144}Nd$	± 2 S.E.	eps (0)	T_{DM}[c] [Ga]	eps (zircon age)	eps (D2; 3200 Ma)
GGM																					
99/111	Mpageni GGM	S25°30'41"/E031°12'47"	2740	0.4711	9.34	0.0071	0.281260	0.000053	-3.7	3.14	-4.6		18.943	14.33	0.0799	0.510290	0.000045	0.5	3.10	-4.6	

								6	7											7	0										
																					9										
																					0										
								0.	0.											0.	.										
								2	0											5	0										
9	Nel	S25°3		0		0.	2	8	0	-					2	0.	1	0	-												
9/	spr	3'56''	3	.	6	0	8	1	0	6	3		3	7	0	0	0	4	3												
1	uit	/E03	1	1	.	0	0	0	0	2	.	-	.	.	7	0	0	9	.	-												
1	GG	0°58'	0	9	2	4	0	0	0	.	3	2.	4	7	5	7	1	.	2	1.												
0	M	14''	6	2	9	3	8	8	8	8	1	3	4	1	1	8	1	8	2	4												
																	0														
								0.	0.											0.	.										
								2	0											5	0										
9	Nel	S25°3		0		0.	2	8	0	-					2	0.	1	0	-												
9/	spr	1'20''	3	.	4	0	8	0	0	6	3		2	4	0	0	0	4	3												
1	uit	/E03	1	1	.	0	0	9	0	5	.	-	.	.	9	1	0	2	.	-												
1	GG	1°19'	0	2	5	3	4	0	8	.	2	1.	3	4	6	7	1	.	2	2.												
2	M	53''	6	6	6	9	5	8	1	6	0		0	5	.	0	8	1	9	2												
																	0														
								0.	0.											0.	.										
								2	0											5	0										
9	Nel	S25°2		0		0.	2	8	0	-					3	0.	1	0	-												
9/	spr	9'30''	3	.	4	0	0	0	0	6	3		5	5	0	0	0	4	3												
1	uit	/E03	1	0	.	0	8	0	0	8	.	-	.	.	9	5	0	0	.	-												
1	GG	1°11'	0	8	8	2	5	1	.	3	2.		7	2	9	4	1	.	2	1.												
8	M	00''	6	4	8	4	9	5	1	2	4		7	9	1	8	0	6	7	8												
																	0														
								0.	0.											0.	.										
								2	0											5	0										
9		S25°3		0		0.	2	8	0	-					2	0.	1	0	-												
9/	Ste	7'04''	3	.	3	0	2	0	0	2	3		3	1	1	0	0	3	3												
1	ntor	/E03	1	5	.	2	0	0	0	3	.	-	.	.	1	7	0	6	.	-												
1	GG	1°18'	0	2	3	2	6	1	.	4	1.		8	0	0	4	1	.	3	2.												
7	M	23''	7	0	4	0	7	1	4	1	0		4	6	2	3	5	8	4	5												
																	0														
								0.	0.											0.	.										
	Bos							2	0							1				5	0										
9	ma	S26°0		0	1	0.	2	8	0	-					1	1	0.	1	-												
9/	nsk	1'14''	3	.	2	0	0	0	0	6	3		1	9	5	1	0	3	3												
1	op	/E03	1	3	.	0	0	9	0	4	.	-	.	.	0	6	0	8	.	-												
2	GG	0°40'	0	7	8	3	7	1	.	3	1.		0	2	0	4	0	.	1	0.												
4	M	34''	7	9	2	7	2	1	1	1	7		8	3	1	4	9	7	8	3												
																	0														
								0.	0.											0.	.										
								2	0											5	0										
9	Mp	S26°0		0		0.	2	8	0	-					1	0.	1	0	-												
9/	uluz	9'17''	3	.	4	0	1	0	0	5	3		3	5	1	0	0	3	3												
1	i	/E03	1	2	.	0	1	0	0	7	.	-	.	.	1	8	0	4	.	-												
2	GG	0°51'	0	2	4	7	6	0	.	2	0.		0	9	6	8	0	.	3	2.												
6	M	36''	7	9	3	3	8	7	2	7	9		6	3	3	1	8	1	3	2												
																	0														
								0.	0.											0.	.										
								2	0							1				5	0										
9	Mp	S26°1		0		0.	2	8	0	-					1	0.	1	0	-												
9/	uluz	2'37''	3	.	9	0	1	0	0	5	3		1	7	9	0	0	4	3												
1	i	/E03	1	4	.	0	1	0	0	8	.	-	.	.	2	4	0	1	.	-												
2	GG	0°35'	0	0	3	6	2	0	.	2	0.		0	6	5	4	1	.	2	1.												
7	M	04''	7	9	8	2	2	8	8	6	9		6	5	4	7	1	8	3	1												

99/115	Salisbury Kop GGM	S25°27'27''/E031°37'34''	3109	0.189	3.76	0.0071	0.281203	0.000008	-55.9	3.23	0.0		5.47	32.34	0.1021	0.510666	0.000009	-38.3	3.21	-0.7	
99/119	Nelspruit GGM	S25°23'34''/E030°58'52''	3109	0.283	6.78	0.0059	0.281118	0.000010	-58.9	3.25	-0.5		8.20	53.80	0.0921	0.510447	0.000012	-42.6	3.22	-1.0	
99/108	Dalmein GGM	S26°04'54''/E030°55'58''	3216-3218	0.223	4.24	0.0074	0.281197	0.000017	-56.2	3.27	1.1		7.77	49.69	0.0945	0.510446	0.000017	-42.6	3.28	-0.5	
Kaap Valley domain																					
99/106	Nelshoogte TTG	S25°51'06''/E030°41'59''	3212-3236	0.049	3.17	0.0022	0.280930	0.000014	-65.6	3.19	3.3		1.88	14.62	0.0779	0.510015	0.000013	-51.0	3.35	2.0	
99/128	Kaap Valley TTG	S25°46'47''/E031°03'24''	3223-3229	0.115	1.60	0.0102	0.281318	0.000015	-51.9	3.36	-0.5		3.06	15.70	0.1177	0.510910	0.000012	-33.5	3.33	-1.0	
Stolzburg domain																					
99/107	Theespruit TTG	S26°02'00''/E030°50'31''	3437-3470	0.081	3.46	0.0033	0.280745	0.000010	-72.1	3.54	-1.0	-6.2	2.02	9.84	0.1243	0.510895	0.000036	-33.8	3.58	-2.0	-4.3
99/121	Theespruit TTG	S26°03'00''/E030°51'46''	3437-3	0.076	3.11	0.0034	0.2808	0.0000	-67.4	3.37	3.4	-1.8	2.08	11.36	0.1107	0.51006	0.000	-39.1	3.51	-1.2	-4.0

			4				7	2								2	0						
			7				9	6								4	1						
			0														9						
			3														0						
			4				0.	0.								0.	.						
			3				2	0								5	0						
9		S26°01'27''/E030°45'41''	1-	0		0.	8	0	-					2	0.	1	0	-					
9/1	Stolzburg		3	.	3	0	0	0	7	3			3	1	1	0	0	4	3				
2			4	0	.	0	8	0	0	.		-	.	.	0	5	0	1	.		-			
0	TTG		6	6	3	2	0	1	.	4	2.	3.	5	5	0	0	2	.	3	1.	2.		
			0	8	3	9	3	0	1	2	3	3	9	3	8	5	0	5	7	1	2		
			3														0						
			4				0.	0.								0.	.						
			2				2	0								5	0						
9		S26°10'33''/E030°59'51''	1-	0		0.	8	0	-					1	0.	1	0	-					
9/1	Steynsdorp		3	.	4	0	1	0	5	3			2	2	1	1	0	2	3				
0			5	2	.	0	1	0	8	.		-	.	.	3	2	0	7	.	-	-		
9	TTG		3	3	6	7	2	1	.	3	4.	0.	7	3	.	0	1	.	5	0.	2.		
			3	1	5	0	3	2	8	5	9	9	8	8	-	9	4	7	0	3	8		
			3														0						
			4				0.	0.								0.	.						
			2				2	0								5	0						
9		S26°11'00''/E030°40'34''	1-	0		0.	8	0	-					1	0.	1	0	-					
9/1	Steynsdorp		3	.	6	0	0	0	6	3			3	7	1	1	0	3	3				
2			5	1	.	0	9	0	5	.		-	.	.	2	0	0	0	.		-			
2	TTG		5	7	1	4	3	0	.	3	5.	1.	5	0	4	6	1	.	3	1.	1.		
			3	8	1	1	3	7	5	5	1	3	3	7	9	0	0	6	5	6	3		

All uncertainties are given as 2 S.E. to the last significant digits

[a] age compilation based on Amelin et al (2000), Armstrong et al (1990), de Ronde & Kamo (2000), Moyen (2019), Kamo & Davis (1994), Kröner et al (1996), Laurent et al (2020), Poujol et al (2003), Schoene et al (2008), Wang et al (2020) and Zeh et al (2009)

[b] T_{DM} calculated assuming linear DM evolution with present-day values of $^{176}Lu/^{177}Hf$ of 0.040 and ε(Hf) of 16.4 (Vervoort et al 2006) using ^{176}Lu of $1.867*10^{-11}a^{-1}$ (Scherer et al. 2001) and chondritic values from Bouvier et al (2008)

[c] T_{DM} calculated assuming linear DM evolution with present-day values of $^{147}Sm/^{144}Nd$ of 0.22 and ε(Nd) of 10.4 (Goldstein et al 1984) using ^{147}Sm of $6.54*10^{-12}a^{-1}$ and chondritic values from Bouvier et al (2008)

Table 2: Mineral Lu-Hf and Sm-Nd isotope data for samples 99/107 (Theespruit TTG) and 99/109 (Steynsdorp TTG)

Steynsdorp pluton 99/109	**comment**	**Lu [µg/g]**	**Hf [µg/g]**	**$^{176}Lu/^{177}Hf$**	**$^{176}Hf/^{177}Hf$**	**Sm [µg/g]**	**Nd [µg/g]**	**$^{147}Sm/^{144}Nd$**	**$^{143}Nd/^{144}Nd$**
titanite-1	400-250µm +	44.6	42.9	0.1470	0.289779 ±5	991	160	0.2173	0.512962 ±5
titanite -2	250-160µm +	47.1	44.0	0.1510	0.289961 ±5	1021	171	0.2134	0.512872 ±7

titanite -3	400-250µm -	39.7	41.6	0.1350	0.288987 ±5	793	152	0.2095	0.512814 ±8
titanite -4	250-160µm -	38.9	40.1	0.1380	0.289179 ±7	692	115	0.2056	0.512725 ±6
amphibole-1	250-160µm	0.396	4.66	0.0120	0.281421 ±7	7.30	43.6	0.1090	0.510679 ±6
amphibole-2	250-160µm					6.73	34.7	0.1212	0.510924 ±7
apatite	250-160µm					303	115 5	0.1583	0.511706 ±14
Theespruit pluton 99/107									
titanite -1	400-250µm +	24.4	39.3	0.0879	0.286244 ±6	944	320 5	0.1780	0.512162 ±6
titanite -2	250-160µm +	23.6	37.1	0.0902	0.286393 ±6	876	295 7	0.1767	0.512130 ±4
titanite -3	160-125µm +	21.5	36.6	0.0832	0.285914 ±8	763	261 6	0.1750	0.512098 ±5
titanite -4	250-160µm -	8.44	25.6	0.0467	0.283578 ±7				
titanite -5	400-250µm +	25.4	46.1	0.0779	0.285615 ±5				
epidote	160-125µm	0.257	7.14	0.0051	0.280903 ±7	11.3	61.2	0.1118	0.510780 ±4
amphibole-1	160-125µm	0.233	8.46	0.0039	0.280849 ±4				
amphibole-2	160-125µm	0.218	7.44	0.0041	0.280848 ±4	6.77	29.6	0.1382	0.511249 ±5
biotite-1	400-250µm +	*0.090*	*6.63*	*0.0019*	*0.280639 ±6*	*0.459*	*1.47*	*0.1893*	*0.511579 ±51*
biotite-2	250-160µm +	*0.107*	*3.64*	*0.0041*	*0.280645 ±15*	*0.998*	*6.63*	*0.0910*	*0.510039 ±16*
biotite-3	250-160µm +	*0.077*	*38.8*	*0.0003*	*0.280687 ±30*				
apatite	400-250µm					39.1	148	0.1603	0.511768 ±5

Given uncertainties are 2 S.E. and correspond to the last significant digit. Uncertainties on $^{147}Sm/^{144}Nd$ and $^{176}Lu/^{177}Hf$ are 0.3% and 1.5% respectively. For isochron calculation the minimum uncertainty on $^{143}Nd/^{144}Nd$ and $^{176}Hf/^{177}Hf$ is given by the external reproducibility of the measured standard values. Values given in italic are not included in age calculations. [a] Plus and minus denotes magnetic or non-magnetic behaviour, respectively, during magnetic separation. Biotite-3 and all titanite splits were separated with 20° inclination at 0.8 A on a Frantz magnetic separator. Biotite-2 and biotite-3 were separated with 20° inclination at 0.4 A.

Step	T (°C)	$^{40}Ar_{tot.}$	^{39}Ar	^{38}Ar	^{37}Ar	^{36}Ar	Age [Ma]

Steynsdorp pluton 99/109 (5.05 mg; J = 6.76*10-3; Ar* = 977; K = 0.62; Ca = 7.1;

Cl = 30)

1	780	142.921±0.009	0.2223±0.0003	0.0139±0.0003	0.0871±0.0007	0.01051±0.00011	2992.6±2.1
2	934	88.446±0.010	0.1908±0.0003	0.0039±0.0002	0.4268±0.0014	0.00339±0.00014	2547.5±2.2
3	948	71.413±0.007	0.1189±0.0003	0.0029±0.0003	0.6124±0.0023	0.00163±0.00013	2921.7±3.5
4	963	79.693±0.007	0.1176±0.0003	0.0032±0.0002	0.8082±0.0028	0.00181±0.00012	3100.3±3.2
5	972	77.690±0.005	0.1135±0.0003	0.0034±0.0002	0.8136±0.0032	0.00315±0.00020	3107.7±4.2
6	985	62.048±0.007	0.0894±0.0003	0.0031±0.0003	0.6589±0.0031	0.00100±0.00013	3139.4±5.5
7	996	43.987±0.004	0.0639±0.0002	0.0014±0.0002	0.4754±0.0020	0.00270±0.00017	3107.6±4.7
8	1016	34.700±0.002	0.0484±0.0003	0.0034±0.0004	0.3884±0.0024	0.00315±0.00015	3153.9±8.1
9	1035	27.153±0.002	0.0360±0.0001	0.0001±0.0003	0.3244±0.0016	0.00193±0.00019	3242.0±6.2
10	1050	27.740±0.002	0.0392±0.0003	0.0027±0.0003	0.3349±0.0021	0.00237±0.00017	3137.5±11.0
11	1070	60.917±0.007	0.0829±0.0003	0.0032±0.0002	0.7441±0.0032	0.00267±0.00019	3212.9±5.2
12	1090	12.176±0.001	0.0161±0.0001	0.0007±0.0003	0.1370±0.0012	0.00280±0.00018	3173.3±14.0
13	1100	10.840±0.001	0.0146±0.0002	0.0009±0.0002	0.1264±0.0021	0.00180±0.00013	3175.7±25.0
14	1110	14.155±0.001	0.0192±0.0002	0.0007±0.0002	0.1625±0.0020	0.00080±0.00021	3212.2±18.0
15	1130	19.488±0.005	0.0266±0.0003	0.0014±0.0003	0.2208±0.0025	0.00142±0.00012	3193.9±16.0
16	1160	27.264±0.002	0.0391±0.0002	0.0036±0.0002	0.3106±0.0017	0.00166±0.00017	3127.0±7.0
17	1190	45.939±0.003	0.0606±0.0001	0.0024±0.0002	0.5154±0.0021	0.00283±0.00017	3253.0±3.9
18	1270	65.087±0.004	0.0871±0.0002	0.0036±0.0002	0.7310±0.0027	0.00128±0.00021	3244.2±3.9
19	1350	68.967±0.006	0.0922±0.0002	0.0011±0.0007	0.7806±0.0027	0.00158±0.00025	3248.8±3.5
20	1400	9.813±0.001	0.0134±0.0003	0.0014±0.0002	0.0971±0.0022	0.00050±0.00025	3198.0±34.0

Theespruit pluton 99/107 small (4.77mg; J = 6.74*10-3; Ar* = 775; K = 0.48; Ca = 5.9; Cl = 104)

1	778	53.587±0.002	0.0835±0.0002	0.0145±0.0002	0.086±0.001	0.0083±0.0001	2942.0±4.1
2	933	56.488±0.004	0.0869±0.0002	0.0095±0.0001	0.433±0.002	0.0034±0.0002	3006.6±4.0
3	953	103.885±0.013	0.1403±0.0003	0.0135±0.0003	0.993±0.003	0.0030±0.0001	3216.4±3.1
4	971	122.725±0.007	0.1664±0.0003	0.0171±0.0003	1.071±0.003	0.0017±0.0001	3216.1±2.5
5	994	54.019±0.003	0.0724±0.0003	0.0078±0.0002	0.446±0.002	0.0027±0.0002	3217.3±5.3
6	1014	21.641±0.001	0.0313±0.0002	0.0030±0.0001	0.196±0.001	0.0019±0.0002	3087.2±10.0

7	102 9	16.527±0.004	0.0206±0.000 7	0.0030±0.000 2	0.159±0.005	0.0019±0.000 2	3295.8±5 1.0
8	104 9	18.815±0.002	0.0258±0.000 2	0.0028±0.000 2	0.184±0.002	0.0014±0.000 1	3173.8±1 2.0
9	106 8	29.770±0.002	0.0401±0.000 1	0.0030±0.000 3	0.284±0.001	0.0015±0.000 2	3211.4±5. 1
10	108 0	32.600±0.003	0.0446±0.000 1	0.0053±0.000 2	0.314±0.001	0.0019±0.000 2	3184.1±5. 1
11	110 0	23.989±0.003	0.0304±0.000 3	0.0030±0.000 2	0.230±0.002	0.0038±0.000 2	3255.0±1 3.0
12	111 0	20.686±0.002	0.0279±0.000 2	0.0029±0.000 2	0.205±0.002	0.0024±0.000 1	3177.9±1 0.0
13	113 0	19.606±0.002	0.0261±0.000 2	0.0031±0.000 2	0.189±0.001	0.0031±0.000 1	3181.2±1 1.0
14	115 0	15.900±0.002	0.0218±0.000 2	0.0038±0.000 1	0.154±0.001	0.0027±0.000 2	3127.4±1 2.0
15	117 0	22.093±0.002	0.0304±0.000 1	0.0027±0.000 2	0.209±0.001	0.0017±0.000 1	3102.5±6. 3
16	120 0	6.416±0.001	0.0079±0.000 2	0.0004±0.000 2	0.065±0.001	0.0018±0.000 2	3244.1±3 3.0
17	124 0	15.093±0.002	0.0207±0.000 2	0.0019±0.000 2	0.142±0.001	0.0019±0.000 2	3153.6±1 2.0
18	127 0	27.612±0.003	0.0370±0.000 2	0.0047±0.000 3	0.282±0.002	0.0024±0.000 1	3202.2±7. 8
19	134 0	95.935±0.007	0.1288±0.000 2	0.0134±0.000 2	0.915±0.003	0.0024±0.000 2	3226.3±2. 5
20	139 0	34.165±0.004	0.0450±0.000 2	0.0035±0.000 2	0.325±0.002	0.0033±0.000 2	3224.7±6. 2

Theespruit pluton 99/107 large (4.38 mg; J = 6.7*10^-3; Ar* = 725; K = 0.61; Ca = 7.0; Cl = 126)

1	765	73.149±0.002	0.1067±0.000 3	0.0185±0.000 2	0.0704±0.000 6	0.0116±0.000 2	3046.5±4. 1
2	929	66.846±0.005	0.1027±0.000 2	0.0088±0.000 2	0.4125±0.001 3	0.0046±0.000 2	2932.1±2. 6
3	943	99.472±0.010	0.1398±0.000 2	0.0144±0.000 2	0.8926±0.002 9	0.0058±0.000 2	3153.9±2. 5
4	955	66.206±0.04	0.0897±0.000 2	0.0084±0.000 2	0.6098±0.002 3	0.0024±0.000 2	3218.9±4. 2
5	966	71.142±0.005	0.0964±0.000 2	0.0088±0.000 3	0.6156±0.002 2	0.0030±0.000 2	3215.9±3. 1
6	981	53.560±0.004	0.0727±0.000 3	0.0070±0.000 2	0.4394±0.002 0	0.0018±0.000 1	3215.3±5. 5
7	993	32.062±0.003	0.0440±0.000 4	0.0049±0.000 3	0.2704±0.002 6	0.0028±0.000 1	3174.5±1 4.0
8	101 2	21.9121±.001	0.0314±0.000 3	0.0028±0.000 3	0.1960±0.001 7	0.0024±0.000 2	3104.3±1 3.0
9	102 4	20.2211±.002	0.0284±0.000 2	0.0030±0.000 2	0.1929±0.001 3	0.0024±0.000 2	3125.4±9. 6
10	104 0	22.775±0.002	0.0314±0.000 2	0.0026±0.000 2	0.2194±0.001 5	0.0016±0.000 2	3178.1±1 0.0
11	106 0	35.564±0.003	0.0473±0.000 2	0.0051±0.000 3	0.3404±0.001 9	0.0027±0.000 2	3229.0±7. 8
12	107 0	47.983±0.004	0.0642±0.000 3	0.0058±0.000 2	0.4456±0.002 4	0.0036±0.000 2	3220.4±6. 9
13	109	41.673±0.004	0.0554±0.000	0.0042±0.000	0.4017±0.001	0.0015±0.000	3248.6±4.

	0		2	2	7	2	9
	111		0.0422±0.000	0.0044±0.000	0.2980±0.002	0.0025±0.000	3173.0±1
14	0	30.624±0.002	3	2	3	2	0.0
	112		0.0338±0.000	0.0039±0.000	0.2430±0.002	0.0017±0.000	3190.5±1
15	0	24.728±0.002	3	2	0	2	2.0
	116		0.0302±0.000	0.0047±0.000	0.2113±0.001	0.0022±0.000	3118.6±9.
16	0	21.275±0.002	2	3	5	2	4
	119		0.0170±0.000	0.0027±0.000	0.1075±0.001	0.0022±0.000	3004.1±1
17	0	11.405±0.002	1	3	0	2	3.0
	127		0.0416±0.000	0.0038±0.000	0.2726±0.001	0.0021±0.000	3146.9±6.
18	0	29.527±0.003	2	3	4	2	9
	134		0.1260±0.000	0.0135±0.000	0.8671±0.002	0.0039±0.000	3242.3±2.
19	0	94.938±0.012	2	3	7	2	5
	138		0.0516±0.000	0.0052±0.000	0.3631±0.001	0.0030±0.000	3235.2±6.
20	0	38.956±0.003	2	2	8	2	3

Table 3: Amphibole Ar-Ar stepwise heating results. All Ar concentrations are given in pL. Uncertainties are on the 1 sigma level. Ar* denotes total ^{40}Ar minus present-day atmospheric ^{40}Ar; integrated K and Ca concentrations are given in %; Cl is given in µg/g. These values are calculated from the total ^{39}Ar, ^{37}Ar and ^{38}Ar, the production ratios and the irradiation time

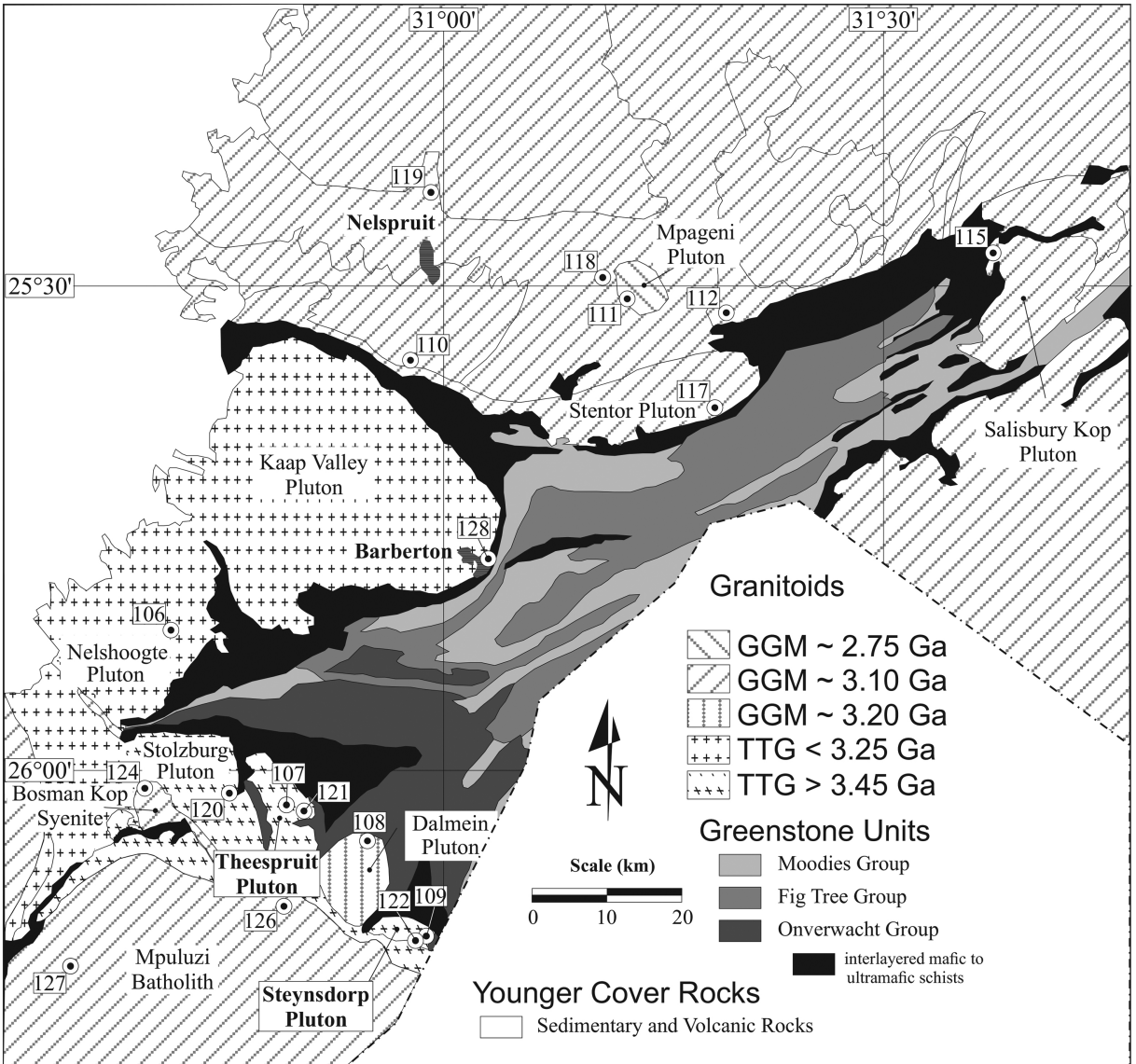
31°00'
31°30'
25°30'
26°00'
119
Nelspruit
118
Mpageni Pluton
111
112
115
110
117
Stentor Pluton
Salisbury Kop Pluton
Kaap Valley Pluton
128
Barberton
106
Nelshoogte Pluton
Stolzburg Pluton
124
107
121
Bosman Kop Syenite
120
108
Dalmein Pluton
Theespruit Pluton
122
109
126
127
Mpuluzi Batholith
Steynsdorp Pluton
Granitoids
GGM ~ 2.75 Ga
GGM ~ 3.10 Ga
GGM ~ 3.20 Ga
TTG < 3.25 Ga
TTG > 3.45 Ga
N
Scale (km)
0
10
20
Greenstone Units
Moodies Group
Fig Tree Group
Onverwacht Group
interlayered mafic to ultramafic schists
Younger Cover Rocks
Sedimentary and Volcanic Rocks

Figure 1

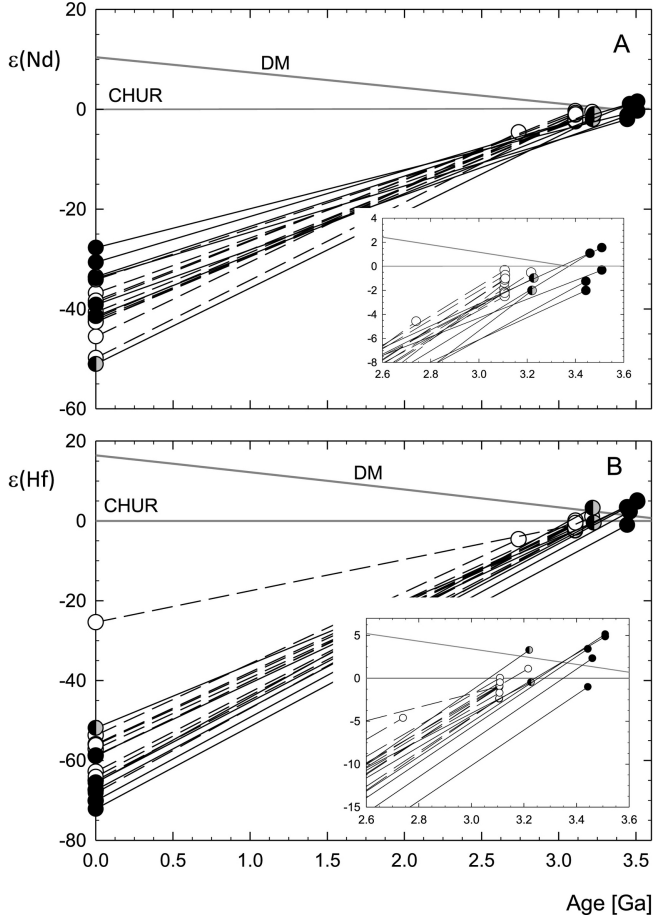
A
ε(Nd)
DM
CHUR
20
0
-20
-40
-60
4
2
0
-2
-4
-6
-8
2.6
2.8
3.0
3.2
3.4
3.6
B
ε(Hf)
DM
CHUR
20
0
-20
-40
-60
-80
5
0
-5
-10
-15
0.0
0.5
1.0
1.5
2.0
2.5
3.0
3.5
Age [Ga]

Figure 2

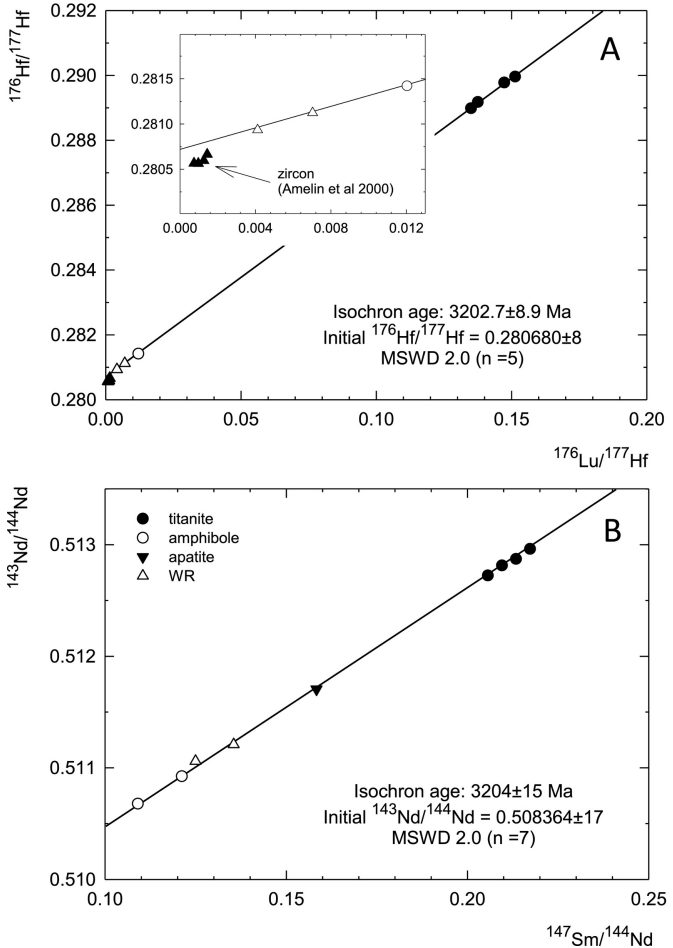
A
$^{176}Hf/^{177}Hf$
$^{176}Lu/^{177}Hf$
0.292
0.290
0.288
0.286
0.284
0.282
0.280
0.00
0.05
0.10
0.15
0.20
0.2815
0.2810
0.2805
zircon
(Amelin et al 2000)
0.000
0.004
0.008
0.012
Isochron age: 3202.7±8.9 Ma
Initial $^{176}Hf/^{177}Hf$ = 0.280680±8
MSWD 2.0 (n =5)
B
titanite
amphibole
apatite
WR
$^{143}Nd/^{144}Nd$
$^{147}Sm/^{144}Nd$
0.513
0.512
0.511
0.510
0.10
0.15
0.20
0.25
Isochron age: 3204±15 Ma
Initial $^{143}Nd/^{144}Nd$ = 0.508364±17
MSWD 2.0 (n =7)

Figure 3

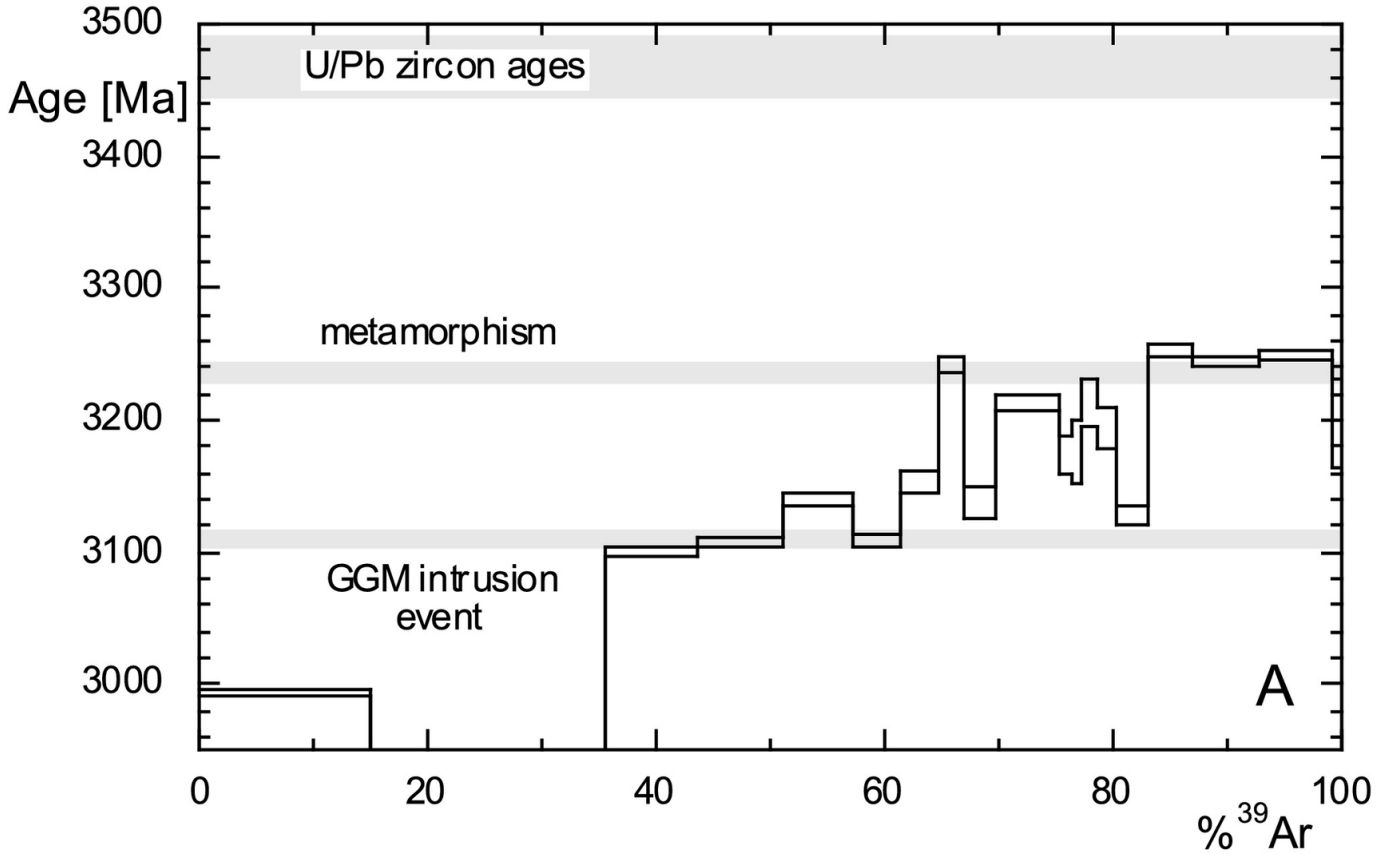
3500
Age [Ma]
3400
3300
3200
3100
3000
U/Pb zircon ages
metamorphism
GGM intrusion
event
A
0
20
40
60
80
100
% 39 Ar

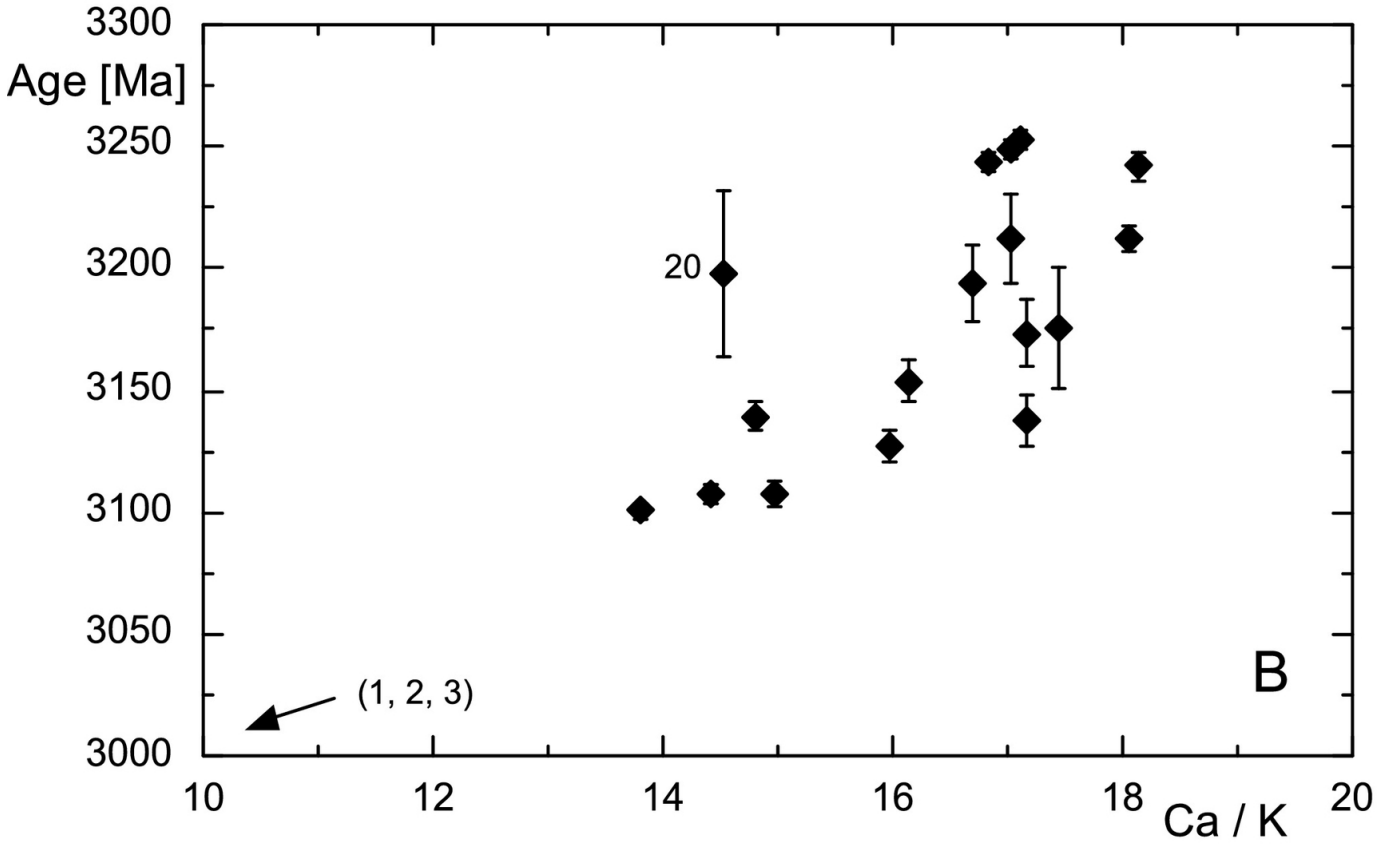
3300
Age [Ma]
3250
3200
3150
3100
3050
3000
20
(1, 2, 3)
B
10
12
14
16
18
20
Ca / K

Figure 4

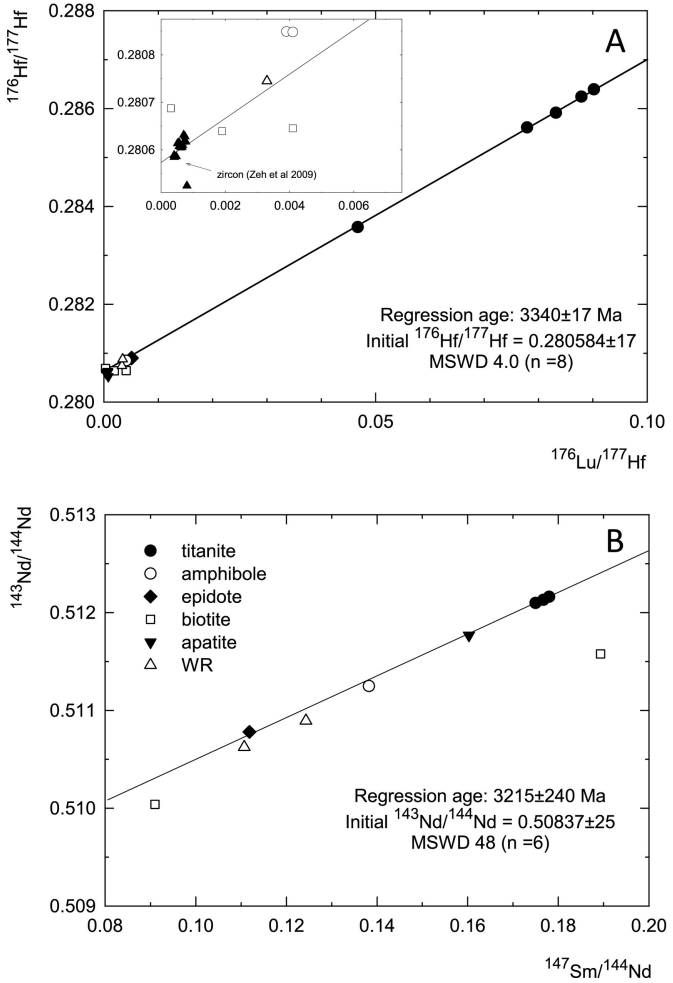
A
$^{176}Hf/^{177}Hf$
$^{176}Lu/^{177}Hf$
0.288
0.286
0.284
0.282
0.280
0.00
0.05
0.10
0.2808
0.2807
0.2806
0.000
0.002
0.004
0.006
zircon (Zeh et al 2009)
Regression age: 3340±17 Ma
Initial $^{176}Hf/^{177}Hf$ = 0.280584±17
MSWD 4.0 (n =8)
B
$^{143}Nd/^{144}Nd$
$^{147}Sm/^{144}Nd$
titanite
amphibole
epidote
biotite
apatite
WR
0.513
0.512
0.511
0.510
0.509
0.08
0.10
0.12
0.14
0.16
0.18
0.20
Regression age: 3215±240 Ma
Initial $^{143}Nd/^{144}Nd$ = 0.50837±25
MSWD 48 (n =6)

Figure 5

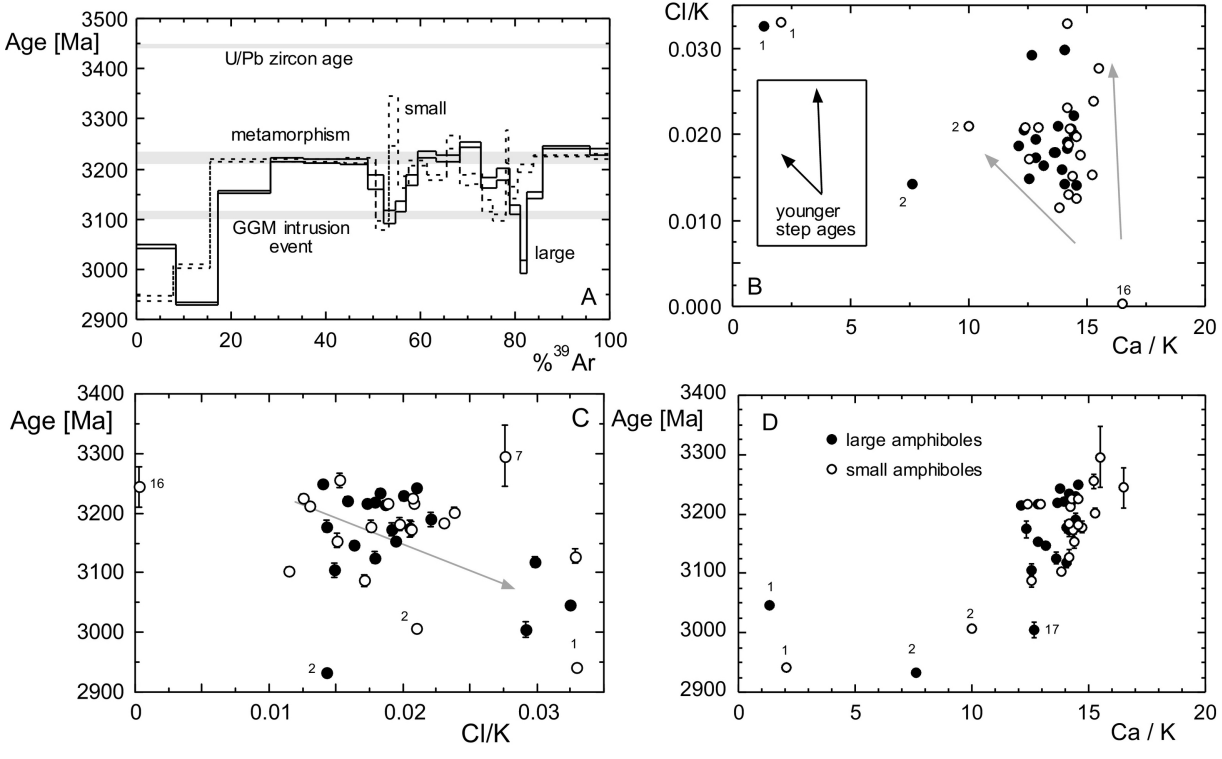
Age [Ma]
U/Pb zircon age
metamorphism
GGM intrusion event
small
large
A
%39Ar
Cl/K
younger step ages
B
Ca / K
C
Age [Ma]
Cl/K
D
large amphiboles
small amphiboles
Ca / K

Figure 6

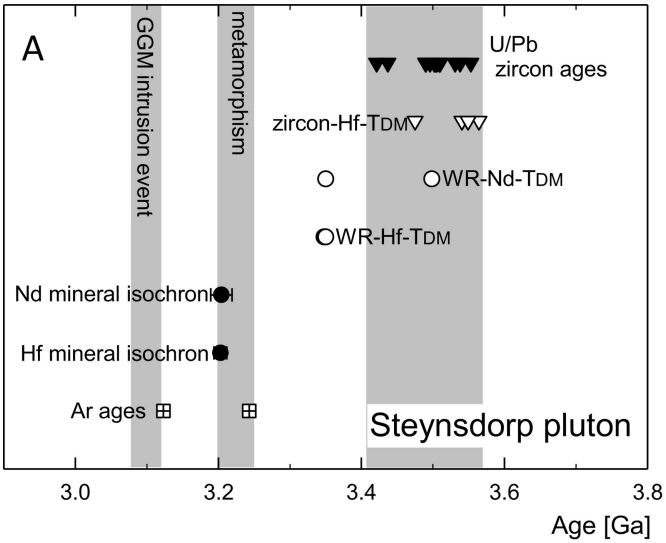
A
GGM intrusion event
metamorphism
U/Pb
zircon ages
zircon-Hf-TDM
WR-Nd-TDM
WR-Hf-TDM
Nd mineral isochron
Hf mineral isochron
Ar ages
Steynsdorp pluton
3.0
3.2
3.4
3.6
3.8
Age [Ga]

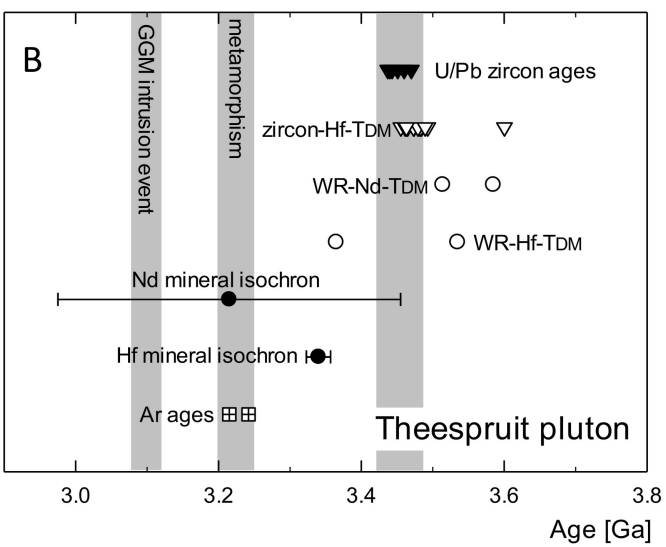
B
GGM intrusion event
metamorphism
U/Pb zircon ages
zircon-Hf-TDM
WR-Nd-TDM
WR-Hf-TDM
Nd mineral isochron
Hf mineral isochron
Ar ages
Theespruit pluton
3.0
3.2
3.4
3.6
3.8
Age [Ga]

Figure 7